JOURNAL OF APPLIED PHYSICS **113**, 174907 (2013)

The nature of chemical reaction-driven tip-streaming

H. C. Mayer and R. Krechetnikov
Department of Mechanical Engineering, University of California, Santa Barbara, California 93106, USA

(Received 15 January 2013; accepted 3 April 2013; published online 6 May 2013)

The discovery of chemical reaction-driven tip-streaming (also known as "an amazing drop") was made about a decade ago during measurements of the dynamic interfacial tension of a water-alkali pendant droplet immersed in oil-linoleic acid. A plausible explanation for this self-sustained ejection of micron sized droplets from the tip of the macroscopic pendant drop was offered at that time and attributed to Marangoni stresses driving the reaction-produced surfactant along the interface. Later, asymptotic theory based on the analysis of a complete fluid dynamical formulation supported this hypothesis. As this discovery promised a way of microdroplet generation without the need for complex microchannel geometries or externally imposed flow or electric fields, we were recently motivated to study the influence of the reagent concentrations and reaction rate on the droplet generation. However, in an attempt to recreate the original experiments, we revealed that the cause for tip-streaming is not what it originally seemed to be. This led to a series of experiments clarifying the role of the Marangoni stresses and the crucial differences from similar phenomena. As the mechanism by which the phenomenon was originally thought to operate was supported by recent theoretical studies, the present work leads to new intriguing questions of existence and conditions under which a chemical reaction alone can drive Marangoni stresses capable of self-sustaining the process of tip-streaming. © *2013 AIP Publishing LLC*. [http://dx.doi.org/10.1063/1.4802497]

I. INTRODUCTION AND MOTIVATION

The formation of microdroplets[1,2] is of vital importance in fields such as chemistry and biology, which nowadays take advantage of miniaturization and compartmentalization,[3] with a variety of applications such as controlled drug delivery, encapsulation of DNA and protein, as well as clinical and environmental field testing, to name a few. It is not only their small volumes but also monodispersity and high frequency of production that make microdroplets indispensable for emerging technologies that require reduced reagent consumption, rapid mixing, continuous processing, and high throughput.[4]

At present, microfluidic methods of droplet formation help to overcome the inherent drawback—the polydispersity in droplet size[5]—of bulk methods to produce microdroplets such as industrial homogenizers. The microfluidic approaches employ monolithic microchannel geometries,[6,7] of which two most commonly studied are the T-junction and the flow focuser.[5] In both cases, droplet dimension is controlled by the geometry and dimensions of the channels, as well as the flow rates of the dispersed and continuous phases. In general, most methods developed over the years for the formation of microdroplets make use of either mechanically imposed flow fields[8] or DC[9–11] and AC[12–14] electric fields. Therefore, droplet formation by different means, without recourse to externally imposed fields (flow or electric), can be desirable, especially if there is a need for self-sustained devices or if samples are sensitive to stresses due to externally imposed fields.

A. Chemical-reaction driven tip-streaming

In this context, the peculiar observation of the spontaneous motion of a water-alkali pendant drop at the tip of a capillary in the oil-acid environment reported by Fernandez and Homsy[15] (FH) was a promising finding, cf. Figure 1, named chemical reaction-driven tip-streaming (CRDTS). By their account, the drop oscillated in a self-sustained fashion, emitting small droplets[16] without any externally imposed flow field.

The discovery of CRDTS was made in the course of dynamic interfacial tension measurements of a water-alkali pendant drop immersed in a paraffin oil-acid mixture. In the physical problem at hand, a chemical reaction at the interface between two phases—less viscous phase 1 in the pendant drop (water + alkali, sodium hydroxide NaOH) and surrounding more viscous phase 2 (oil + linoleic acid)—produces a nearly insoluble surfactant,[17,18,91,92] cf. Figure 1,

$$\underset{\text{linoleic acid}}{RO^-} + H^+ + \underset{\text{sodium hydroxide}}{Na^+ + HO^-} \rightarrow H_2O + RO^-Na^+,$$

where it is assumed that recombination of H^+ and HO^- and that of Na^+ and RO^- dominate any other. As a possible explanation of the observed phenomena, it was suggested by FH and Krechetnikov and Homsy[19] (KH) that the surfactant ends up being distributed non-uniformly along the interface in a self-sustained fashion, which drives Marangoni flow in both phases and sweeps surfactant towards the tip of the conical drop. The resulting low interfacial tension in the tip area allows the interface to elongate and to create a thin thread, cf. Figure 1(e), through which the phase 1 is ejected into phase 2. The process was thought to be initiated by the detachment of a large water-alkali pendant drop from the tip of the capillary, cf. Figures 1(a)–1(c), due to the reduction in interfacial tension to a value insufficient to balance the weight of the suspended water-alkali drop. This *first drop* gives rise to an initial extensional flow in the oil phase,

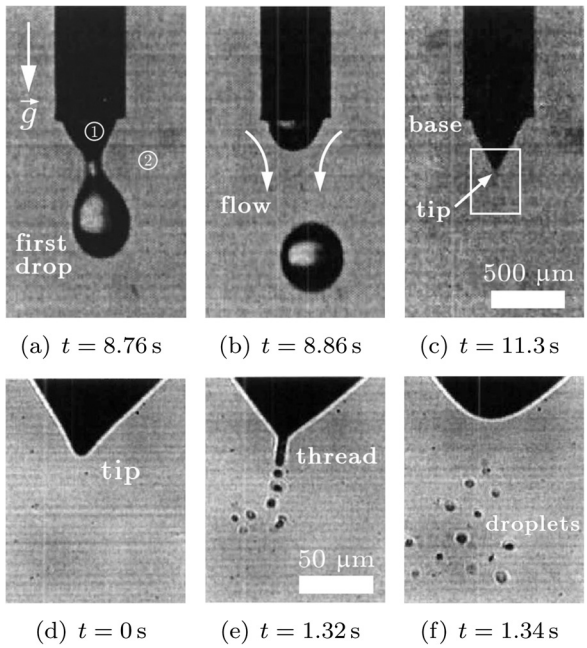

FIG. 1. CRDTS observations by Fernandez and Homsy:[15] (a)-(c) the detachment of the initial pendant drop followed by the formation of a cone shape with a pointed end; (d)-(f) a magnified view of droplet formation near the drop tip for one period in the oscillatory mode, indicated approximately by the box in Figure 1(c). Reprinted with permission from J. M. Fernandez and G. M. Homsy, "Chemical reaction-driven tip-streaming phenomena in a pendant drop," Phys. Fluids **16**, 2548-2555 (2004). Copyright 2004 American Institute of Physics.

which sweeps surfactant to the tip of the liquid remaining on the capillary, cf. Figure 2. Due to the decrease in interfacial tension as a result of surfactant crowding, the tip forms a small thread, which breaks into microscale droplets that carry surfactant away from the interface, cf. Figures 1(d)–1(f) and 2. Next, shedding surfactant-rich droplets from the tip leads to an interfacial tension gradient along the pendant drop interface because of the continued production of surfactant near the base of the capillary. As a result, a Marangoni stress (*not* the initial extensional flow) drives surfactant to the tip, cf. Figure 2, causing crowding and again reducing the interfacial tension. The droplet emission process repeats and was hypothesized to be self-sustaining, i.e., (t)→(i)→(ii)→(iii)→(iv)→(i)→(ii) in Figure 2, so long as reagents producing surfactant are not exhausted.

In their original work, FH discuss two distinct modes of droplet formation. The first is "*self-sustained oscillations*" (SSO), in which the drop at the tip of the capillary periodically

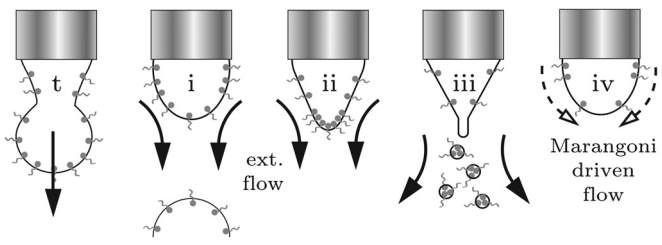

FIG. 2. "*A plausible self-sustaining mechanism*" for CRDTS as proposed by FH[15] and KH.[19]

oscillated from a hemispherical cap to a cone with droplets emitted from the tip of a thread at the cone apex. The oscillations of the interface and the formation of droplets were sustained for approximately 10–20 min with the frequency of the drop oscillations f decreasing with time but typically in the range of $f \sim 0.4 - 2.5\,\mathrm{s}^{-1}$. A second observed mode of droplet formation was termed "*steady tip-streaming*" (ST), in which case the water-alkali drop assumed a steady cone-like shape but with microscale droplets continuously ejected from the tip of the cone, cf. Figure 1(e).

B. Further evidence

A number of arguments have been made to justify the above proposed mechanism.[15,19] First, due to the formation of microscale droplets, the disparity in length scales between the capillary and droplet size (∼100 : 1), the water-oil viscosity ratio ($\mu_1/\mu_2 \sim 0.005$), and the presence of surfactants, FH noted a number of similarities between the CRDTS phenomenon and tip-streaming behavior resulting from mechanically driven flows,[20–22] in particular the form of drop break-up observed by Taylor in a four-roll mill apparatus.[20] Thread elongation rates measured using high-speed imaging resulted in an estimated capillary number of $Ca \sim 0.7$ for the flow field strain rates in the vicinity of the cone tip—favorably close to the critical value $Ca_c \sim 0.5$ necessary for tip-streaming.[8] Thus, FH concluded that this should *imply* that an extensional flow exists in the continuous phase and that "*the flow arises spontaneously as a result of the chemical reaction.*" All these observations and the absence of an externally imposed flow field led FH and KH to believe that both regimes, SSO and ST, resulted from self-sustained tip-streaming driven solely by Marangoni effects.

Moreover, further studies showed the existence of a family of self-similar axisymmetric three-dimensional solutions in the neighborhood of a singularity;[19,23] the resolution of this singularity was achieved via the construction of a thread solution with a singular perturbation technique and matching to the self-similar solution,[23] so that the scaling law for the thread diameter, cf. Figure 1(e), was determined to be

$$d_M \sim l_c \sin\theta\, \sigma_{min}/\sigma_{max}, \tag{1}$$

i.e., controlled by the ratio of interfacial tensions in the cone and thread regions $\sigma_{min}/\sigma_{max}$—the smaller the ratio, the stronger the Marangoni effects and the thinner the thread; here, l_c is the capillary length and θ the cone semi-angle.

KH noticed the apparent similarity of the observed cone shape of the drop in the bursting regime to Taylor cones (TCs).[20,24] While the shape and bursting effects suggest an analogy to the phenomena of formation of stable cones in electrified liquid interfaces, the underlying physical mechanisms behind the TC are different. As explained by Taylor, the conical shape arises due to a balance of normal stresses: the electrostatic pressure $\epsilon_0 E_n^2/2$ induced by the normal component of electrical field E_n (the tangential component being zero in view of the assumed equipotentiality of the interface) equilibrates with the capillary pressure $\sigma \cot\theta/r$, which

varies inversely with the distance from cone tip, r, so that $E_n \sim (\sigma/\epsilon_0 r)^{1/2}$. In the case of Marangoni-driven cones, the conical shape is produced as a result of balancing both normal and tangent stresses, with the predominant role played by the gradient of interfacial tension.

From a practical point of view, the production of surfactant at an interface (as opposed to simply adding surfactant to a system) and resulting Marangoni effects can be harnessed for some particular purpose, e.g., in a microfluidic flow focusing device to modify droplet formation.[25] Thus, further study of these chemically induced Marangoni effects is of value. The original work on CRDTS left a number of important questions unanswered, in particular on the influence of reagent concentrations on the size and frequency of the emitted droplets. While held fixed in the experiments of FH, the reagent concentrations dictate reaction rates and dynamic interfacial tension behavior.[26,27] This and other questions motivated our study.

C. Paper outline

The paper is organized as follows. First, in Sec. II A, we discuss our attempts to recreate the original CRDTS experiments,[15] which led to uncovering its true origin. In Sec. II B, we quantify the determined mechanisms, and in Sec. III, we discuss the relation to the electrospray (ES) phenomena and clarify the role of Marangoni effects. This sequence of experimental and theoretical insights ultimately leads to a number of questions requiring further understanding of these intriguing phenomena to be discussed in Sec. IV.

II. THE TRUE NATURE OF CRDTS

A. Recreating the original CRDTS experiments

We started our re-investigation of the CRDTS phenomenon with an experimental setup nearly identical to that of FH and shown in Figure 3. Polystyrene cuvettes (VWR) of 1 cm × 1 cm cross-section and 5 cm height were used to contain an oil-acid solution made from paraffin oil (heavy mineral oil, Fisher Scientific) and linoleic acid (99% purity, Acros Organics). A blunt stainless steel hypodermic needle[28] (20 gage, 0.91 mm outside diameter, McMaster-Carr) was affixed to a microliter syringe (Hamilton Gastight) and held by a clamp directly above the cuvette. The cuvette could be raised or lowered using a laboratory jack. At the start of each experiment, we filled the cuvette with the oil-acid mixture. The syringe was filled with a water-alkali solution of DI water and sodium hydroxide pellets (98% purity, Fisher Scientific), clamped into position, and then submerged into the oil-acid phase. A pendant drop was formed at the tip of the submerged needle by manually advancing the syringe plunger.

While the same reagent concentrations as reported by FH were initially used (i.e., $C_{NaOH} = 12.5$ mM and $C_{acid} = 1$ mM), we were surprised to find that the modes of droplet formation, either self-sustained oscillations or steady tip-streaming, were not *"robust and repeatable"* as asserted by FH. Only sporadic droplet formation was observed, and

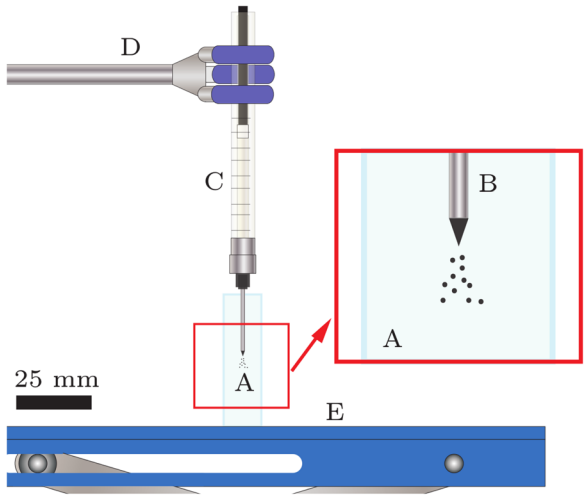

FIG. 3. An attempt at recreating the original CRDTS setup of Fernandez and Homsy.[15] A plastic cuvette (A) is filled with an oil-acid solution, into which a stainless steel needle (B) is submerged; the latter supports a water-alkali drop at its end fed by a Hamilton microliter syringe (C). The syringe is supported by a laboratory clamp (D), and the cuvette can be translated vertically by a scissor jack (E). Droplet emission from the suspended water-alkali drop (see inset) is recorded using a Phantom v5.2 camera and Nikon lens/extension tube set (not shown).

typically these instances occurred immediately after submerging the needle into the oil-acid solution. Very few occasions were encountered where sustained droplet emission occurred over long timescales (i.e., tens of minutes) and none of these events exhibited the drop oscillation frequencies similar to those reported by FH, i.e., $\sim 1\ s^{-1}$.

In a continued attempt to recreate the CRDTS phenomenon, we varied the concentrations of the reagents as well as syringe needle diameter. Still, only sporadic droplet formation was encountered. It was only after numerous attempts at recreating the CRDTS behavior that we made two simple but important observations: (1) after normal handling of the cuvettes (consistent with filling, transporting, and positioning them in the experimental setup), the vertical sidewalls were capable of attracting a piece of laboratory wipe held in their immediate vicinity; (2) tip-streaming was always observed if intentional contact with the sidewall was made while the syringe needle was submerged. In conjunction with the statement by FH that the steady tip-streaming mode was only observed if they *"move the cell horizontally from left to right for a short time (less than 1 min),"* both our findings allude to a radically different cause of the CRDTS phenomenon and point to the potential influence of static charge. This alternate plausible mechanism gives rise to a number of new questions. First, is it probable that the original CRDTS observations were actually the result of inadvertent and unnoticed[29] static charging of the plastic cuvettes? Second, is the magnitude of charge acquired by the cuvette sidewalls during normal handling sufficient to produce any droplet emission from the water-alkali pendant drop via the electrospray mechanism? Third, are the different modes of the drop behavior—self-sustained oscillations and steady tip-streaming—and any transition between them consistent with the variation of the charge magnitudes produced by normal handling of the cuvettes?

B. The influence of static charge

Despite the common occurrence of contact electrification (aka triboelectric charging), and the significant role that charging plays in materials science and technology, the fundamental mechanisms of contact electrification between insulators remain elusive and poorly understood.[30] What makes contact electrification behavior difficult to predict with accuracy is that the magnitude, polarity of charge transfer,[31] and rate of surface charge decay are sensitive to a variety of factors, including material properties, environmental conditions, and the contact process itself.[32,93,94] Therefore, a triboelectric series is a simple arrangement of materials based on observations of charge acquisition after contact and separation[33] as in Table I.

Since we are attempting to recreate the circumstances under which the CRDTS experiments of FH were performed, we have used the standard polystyrene cuvettes from the original experiments as well as typical laboratory glove materials.[35] The ambient conditions are set by the air conditioned laboratory environment: a range of temperature ($22 - 26\,^{\circ}$C) and relative humidity level (39%–55% RH). To replicate the original CRDTS experiments of FH,[15] we also restricted ourselves to what we consider to be normal, or typical, handling of the cuvettes. Table I contains a condensed triboelectric series[36] with the materials that were reported and expected to have been used in the original CRDTS experiments.[15] Recall that in a triboelectric series, a higher positioned material in the table will tend to acquire a positive charge when contacted with a material below it (which will end up acquiring a negative charge).[34] The further apart two materials are in the series, the larger the expected magnitude of charge transfer.

Inspection of the Table I suggests that contact electrification should result in a positive charge transferred to the cuvette sidewall from gloved hands (nitrile, latex, or vinyl) and a negative charge transferred to the cuvette sidewall from a laboratory wipe. While the magnitude of the charge transfer, and hence the effective electrostatic potential of the cuvette sidewall, cannot be determined from the qualitative triboelectric series, the relatively large separation in Table I between cuvette materials and both gloves and laboratory wipes suggests that the magnitude of the charge transferred may be significant and thus makes inadvertent charging during the original CRDTS experiments of FH probable. Determining the magnitude of the transferred charge, or equivalently the electrostatic potential of the cuvette sidewall, and thus answering the question of whether or not static charge is capable of producing droplet formation in the CRDTS system require more than a simple inspection of the triboelectric series and necessitates experimental measurements, which will be presented below.

TABLE I. Triboelectric series for common laboratory materials used in CRDTS experiments.[34]

Positive charge (+)	
Paper	laboratory wipe
...[a]	
Polystyrene (PS)	cuvette materials
Polymethylmethacrylate (PMMA)	
...	
Butadiene-acrylonitrile (nitrile)	glove materials
Natural rubber (latex)	
Polyvinyl chloride (vinyl)	
negative charge (–)	

[a]Continuation notation implies a significant jump between materials in the series, which have been left out here for brevity.

1. Materials and methods

The experimental setup used for quantifying contact electrification and its effects on the modes of droplet formation is shown in Figure 4. Improvements were made over the original setup in Figure 3 to ensure consistent positioning of the syringe needle within the plastic cuvette, as well as providing visual access from the front and side and physical access to the cuvette sidewall for intentional contact electrification and surface potential measurements. The syringe used to dispense water-alkali solution to the tip of the submerged needle was mounted in a precision syringe pump (Ph.D. model, Harvard Apparatus) and connected to the needle via a short section of tubing. This eliminated contact with the syringe needle during the course of experiments. Droplet formation was recorded using a Phantom v5.2 digital high speed camera (VisionResearch) with a 55 mm Nikor lens and extension tube set. The same chemicals (linoleic acid and

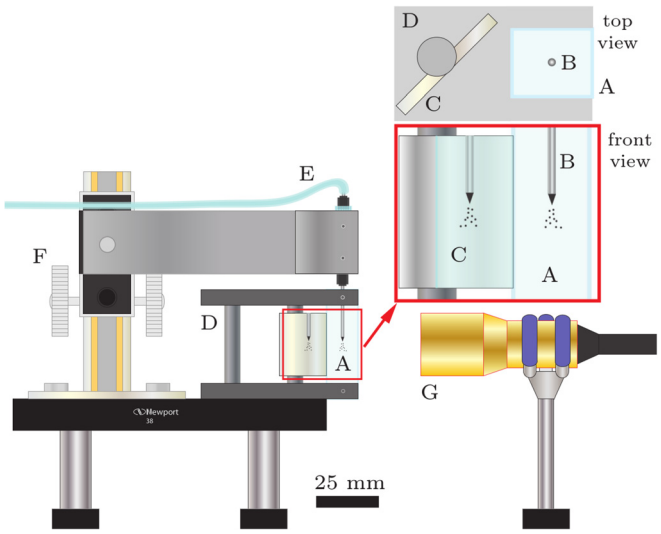

FIG. 4. Modified CRDTS setup to incorporate contact electrification measurements. The setup possesses many of the same features shown in Figure 3 including the plastic polystyrene cuvette (A) with the submerged stainless steel hypodermic needle (B). A mirror (C) is used to simultaneously image the side view of the needle and cuvette. The cuvette and mirror are mounted to the cuvette holder (D). The needle (B) is supported by an arm fixed to the linear stage (F) for raising and lowering. The water-alkali solution is supplied to the needle tip using tube (E) connected to a syringe pump (Harvard Apparatus PhD, not shown). This enables minimal contact between system components and the experiment operator as well as accurate dispensing of liquid. A surface voltmeter (G) is positioned 25 mm from the surface of the cuvette for surface voltage measurements. This arrangement provides sufficient spacing for intentional and controlled contact with the cuvette sidewall. The drop formation at the tip of the needle is illuminated from the back and sides using LED lamps and diffuser plates (not shown) and recorded by a Phantom v5.2 digital high speed camera (not shown).

TABLE II. Properties of water-NaOH and oil-linoleic acid mixtures: interfacial tension σ, conductivity κ, and relative permittivity ϵ_r.

C_{NaOH} [mM]	C_{acid} [mM]	σ_{eq} (Ref. 27) [mN/m]	κ_{NaOH} (Ref. 37) [S/m]	$\epsilon_{r,NaOH}$ (Ref. 38)	$\epsilon_{r,oil}$ (Ref. 39)
0	0	52	5×10^{-6}		
12.5	0.1	18		~85	~2.2
12.5	1.0[a]	3	3×10^{-1}		
12.5	10.0	0.1			

[a]The concentration employed in the original CRDTS experiments by FH.

NaOH) were used to create the range of solutions with the properties presented in Table II.

Measurements of the cuvette sidewall surface potential resulting from contact electrification were performed with a direct current surface voltmeter (Model USSVM, AlphaLabs Inc.). The USSVM is a rotating vane field mill type sensor, which is suitable for measurements over long periods of time[40] without contact and without drainage of surface charge.[41] Since the plastic cuvettes possess a relatively small vertical sidewall area (1 cm wide × 5 cm tall) as compared to the measurement probe head (~2.5 cm diameter), it is expected that the surface potential reading is not the exact value. While for the purposes here—i.e., to confirm that static charge on the outside of the cuvette resulting from contact electrification is responsible for the originally reported CRDTS behavior—it is sufficient to measure relative differences in the magnitude of the surface potential due to changes in contact electrification processes (which is achieved with consistent placement of the measurement probe), we will also be able to get the order of magnitude of the potential of the cell wall based on the following physical consideration.

Because the "voltage" of an insulator is poorly defined,[42] either the total charge Q or the charge per unit area Q/A on the surface is usually measured on a charged insulator. The voltage V_S is approximately proportional to the distance between the grounded object and the insulator's surface L_{meas}, multiplied by the amount of charge per unit area on the surface Q/A consistent with Gauss' law applied to an infinite planar surface with a uniform electric field, i.e., $Q/A = \epsilon_0 E$, where $E = V_S/L_{meas}$ and hence $Q/A = (\epsilon_0/L_{meas})V_S$. For a finite size sample, the displayed voltage will be less than the voltage measured on an infinite sample with the same surface charge density, which can be accounted for with a correction factor.[43]

2. Effect of intentional charging on droplet emission

To demonstrate that contact electrification can result in the droplet formation behavior reported by FH, i.e., either self-sustained oscillations or steady tip-streaming, we recreated the original CRDTS experiments in the presence of a charged cuvette sidewall with the setup in Figure 4. At the start of each experiment, the cuvette was filled with the oil-acid solution ($C_{acid} = 1.0$ mM) and carefully loaded into the cuvette holder. The syringe needle was then lowered into position, submerged in the oil-acid phase, and an $O(1\,\text{mm})$ diameter water-alkali droplet was formed on the tip of the syringe needle (cf. images for $t < 0$ in Figure 5). Contact electrification was then initiated by sliding contact of a glove covered finger with the cuvette sidewall, which magnitude and persistence are quantified in detail in Appendix A. This resulted in a rapid increase in the surface potential V_S, followed by the deformation of the water-alkali drop anchored on the needle and subsequent emission of small droplets from the tip of the drop. This process is presented in Figure 5 relating $V_S(t)$ and the corresponding drop modes.

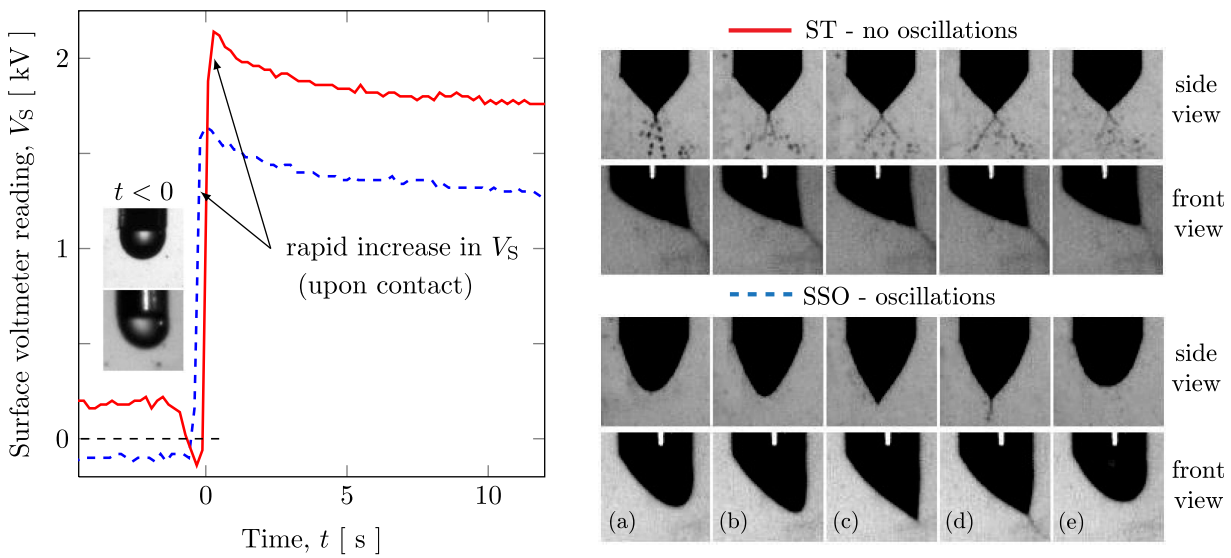

FIG. 5. Evidence of the initiation of both SSO and ST modes resulting from contact electrification of the cuvette sidewall in the case of $C_{NaOH} = 12.5$ mM and $C_{acid} = 1.0$ mM. The magnitude of V_S appears to control the mode type with $V_S(\text{ST}) > V_S(\text{SSO})$. The inset images (a)-(e) include both the side and front views with the corresponding time intervals between frames: $\Delta t_{a-b} = 0.16$ s, $\Delta t_{b-c} = 0.02$ s, $\Delta t_{c-d} = 0.01$ s, and $\Delta t_{d-e} = 0.58$ s. The front view indicates a pull of the interface toward the charged sidewall (which is located on the right hand side of the front view images). This asymmetry is not visible in the side view in which the drop is imaged through the transparent charged surface. For the SSO mode, the images show the oscillation between rounded interface ((a), (b), and (e)) and cone-like interface with a liquid thread at the tip ((c) and (d)). For the ST mode, the images show that there are no oscillations of the interface, but rather a steady cone-like shape persists with small droplets continuously emitted from the cone tip.

The sequences of images in Figure 5 show that for different magnitudes of surface potential, the two modes of drop formation reported by FH can be observed. The lower V_S curve corresponds to the behavior that is similar to self-sustained oscillations—the image sequence labeled SSO shows the same pulsating motion and periodic droplet emission described by FH, cf. Figure 2. An increase in V_S, simply from enhanced contact electrification, results in the steady tip-streaming. From the image sequence ST, it is apparent that the water-alkali drop at the tip of the capillary assumes a steady cone-like shape with small droplets continuously emitted from its tip.

In the set of experiments summarized by Figure 5, we have clearly initiated droplet formation by one intentional contact electrification event. But, in the work of FH, the self-sustained oscillation mode was observed to arise spontaneously after the fall of the first drop. How can we reconcile this difference? The most logical explanation is that in the original experiments of FH, the sidewalls of the cuvette had some static charge as a result of contact electrification, perhaps due to regular handling, which can be significant as follows from the data in Figure 15 in Appendix A. If the needle was submerged without a large water-alkali drop, there may not have been any initial droplet emission upon entry. Yet, after creating a pendant drop on the capillary tip by dispensing water-alkali solution from the syringe, and a reduction in interfacial tension at the oil-water interface owing to the production of surfactant via the chemical reaction, the electric field established by the cuvette surface charge could have been strong enough to detach a large drop (the first drop) and the remaining water-alkali drop at the end of the capillary could then be induced into self-sustained oscillations. In fact, if one carefully inspects the images from FH shown in Figures 1(a) and 1(b), it is apparent that the drop pulled from the needle tip has a bias toward the right side of the image. This bias is likely the result of the charged cuvette sidewall as is also observed in the inset images of Figure 5 (cf. front view images indicating an attraction of the water-alkali tip and droplets to the charged wall; note that side view images recorded orthogonally to the front view do not show this attraction). Now recall that the steady tip-streaming mode described by FH was only observed after contact with the cuvette, cf. the discussion in Sec. II A. Such behavior is consistent with our measurements indicating that increased contact results in increased charge cuvette surface potential and thus a transition from the self-sustained oscillation mode to steady tip-streaming.

Finally, let us support the above arguments that the static electricity on the cuvette wall can induce significant drop deformations with the estimates of the electric Bond number, $Bo_e = \epsilon_{r,NaOH}\,\epsilon_0\,R\,V^2/(\sigma_{eq}H^2)$, a measure of the relative importance of interfacial tension forces to electrical forces acting on a suspended drop.[44] In this definition, ϵ_0 is the electrical permittivity of free space, $\epsilon_{r,NaOH}$ is the relative permittivity of the water-alkali solution, and R is the radius of the drop. We also assume that the magnitude of the electric field strength can be characterized effectively by $E \sim V/H$, where V is the potential difference between a large planar electrode (in this case the cuvette sidewall) placed a distance H away from the capillary tip. Using $R = 0.5$ mm, $H = 5$ mm (half the width of the cuvette), and the properties of the water-alkali solution given in Table II, interfacial tension forces turn out to be of the same order of magnitude as electrical forces, i.e., $Bo_e \sim 1$, for a potential of only $V \sim 500$ V.

Furthermore, as mentioned above, upon closer examination of the photos in Figures 1(a) and 1(b), we can see that the detached first drop does not fall straight down (in line with $\vec{g}$) but drifts, or is attracted, to the right side. This suggests that there was a charge on the right cuvette sidewall when that image was taken. We can also estimate the velocity[45] of the falling drop in Figures 1(a) and 1(b), using the time stamps provided and the needle diameter as a scale bar, to be $U_{fall} \sim 2.5 - 5.0$ mm/s, whereas the terminal velocity of such a drop (water in oil) should only be $U_{term} \sim 0.2 - 0.8$ mm/s based on the Hadamard-Rybczynski equation.[46] Thus, it is obvious that a force other than gravity is causing the drop to move away from the needle after detachment.

3. CRDTS—an inadvertent electrospray

It was originally hypothesized by FH that CRDTS was a self-sustained phenomenon driven by Marangoni stresses, cf. discussion in Sec. I A. While we demonstrated here that it is in fact contact electrification that is responsible for initiating droplet formation, is it possible that contact electrification is only needed to initiate the process and that the surfactant produced by chemical reaction and resulting Marangoni stresses can *sustain* motion? To test this, we performed experiments analogous to that in Figure 5, but the surface potential/charge was eliminated from the cuvette sidewall using an anti-static brush after droplet formation was initiated by a step increase in surface potential. The result of this process is presented in Figure 6, where the measured value of V_S is plotted as a function of time showing the step increase and decrease in surface potential. Inset (a) shows the water-alkali pendant drop prior to the increase in surface potential resulting from sliding contact; in (b), we can see a portion of the gloved finger (bottom of the inset image), which has made sliding contact with the cuvette sidewall resulting in an increase of the surface potential and thus commencing droplet emission by the self-sustained oscillation mode (c)—in the provided image sequence the formation and breakup of the tip thread are visible. Then, the static charge on the cuvette sidewall is essentially removed by sweeping an anti-static brush along the surface, cf. inset (d). With a decrease in surface potential comes a relaxation of the water-alkali drop back to the initial static state (e); however, the size of the drop has been noticeably reduced by the emission of small droplets. It is clear from this sequence that drop formation is not only *initiated* by contact electrification, but *ceases* to occur after the static charge on the cuvette sidewall is removed or reduced to an insignificant value. Although shown in Figure 6 for the case of self-sustained oscillations, we have also observed the same initiation-cessation for the steady tip-streaming regime.

We can now conclude that the original CRDTS phenomenon was *not* a self-sustaining form of droplet emission

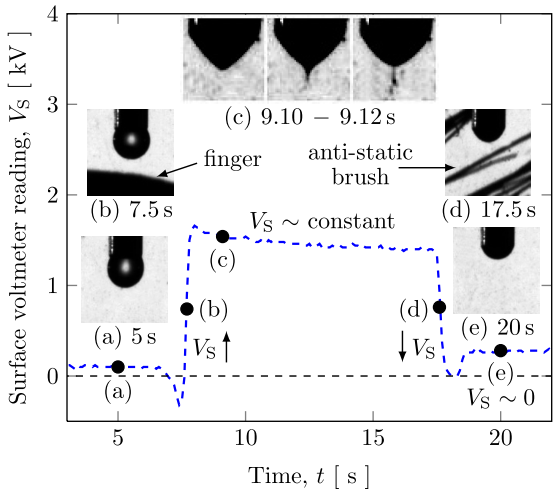

FIG. 6. Visualization of the initiation and termination of droplet emission by control of the cuvette sidewall charge (indicated by the measured potential) for the $C_{NaOH} = 12.5\,mM$ and $C_{acid} = 1.0\,mM$ systems. An initially static pendant drop (a) is exposed to a charged cuvette sidewall by contact electrification (b)—note the gloved finger in the bottom of the image. A droplet is shed from the needle and the remaining drop undergoes self-sustained oscillations (c). Removal of the static charge on the cuvette sidewall is accomplished by wiping with an anti-static brush (d)—note the bristles in the image. After removal of the charge, tip-streaming is effectively terminated (e).

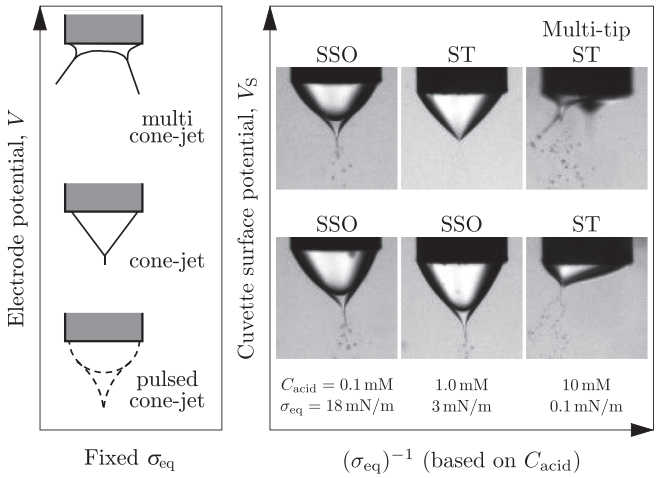

(a) Mode sketches. (b) Images from our experiments.

FIG. 7. Various modes of drop formation[49] observed in ES (a) and compared to modes accessible by contact electrification using the CRDTS system (b). (a) For ES, the transition from pulsed cone-jet to cone-jet to multicone-jet is accomplished at fixed flow rate by an increase in the electrode potential (electric field strength). (b) Similar modes of drop formation are observed for the CRDTS system using contact electrification to adjust the cuvette sidewall surface potential. However in the CRDTS system, changes in reagent concentrations can result in substantial variations of interfacial tension σ_{eq}. These can also be used to produce different spray modes when contact electrification is insufficient to produce the required potential. Note that for the images labeled SSO in (b), two photos have been superimposed to show the oscillation of the interface as suggested in the pulsed cone-jet sketch (a).

driven solely by Marangoni effects as previously believed,[15,19] but rather an inadvertent ES, i.e., liquid atomization caused here by the contact electrification of the cuvette sidewall resulting in a sufficiently strong electric field in the vicinity of the water-alkali drop. In traditional electrosprays, a plethora of different spray modes exists depending on the electric field strength, which are characterized, often qualitatively, by how the sprayed liquid breaks up into droplets.[47–49] Therefore, a comparison of the observations from the CRDTS experiments to the standard ES modes will further strengthen our conclusions regarding the true nature of CRDTS.

The fluid properties relevant for such a comparison are the interfacial tension σ, viscosity μ, permittivity ϵ, and conductivity κ of both the sprayed and ambient fluids. As suggested by the electric Bond number Bo_e, liquids with higher surface tension require stronger electric fields to produce ES. The type of spray modes is also controlled by the conductivity—in this context, it must be noted that the presence of NaOH in the concentrations used in our experiments corresponds to the high conductivity range, based on the standard classification.[50] It is coincidental that the addition of NaOH to water in the CRDTS experiments unintentionally modifies the conductivity. Both effects—increased conductivity and decreased interfacial tension—allow for ES of the water phase using much lower applied potentials than it would be required without NaOH.

In the conventional ES setup, for fixed liquid properties, electrode configuration, and imposed flow rate that replenishes the liquid lost to the spray, an increase in potential V can produce the following sequence of ES modes: pulsed cone-jet, cone-jet, and multi cone-jet as sketched in Figure 7(a). In the *pulsed cone-jet* mode, the interface oscillates between a hemispherical and cone shapes with an ejection of droplets from the tip.[48] In the *cone-jet* mode, the interface maintains a steady conical shape and very small droplets are released from a thread formed at the tip. The cone semi-angle is $\theta_{TC} \sim 49^{\circ}$ for highly conductive liquids, but can vary with the conductivity and permittivity of the sprayed and ambient fluids.[51,52] For V beyond the steady cone-jet mode, the jet can split, forming a number of drop emitting sites around the capillary tip, which is often called the *multi-cone-jet* mode.[49] It should be noted that the transitions between all of these possible modes are generally not well defined except for the TC mode.[48]

Using the previously described CRDTS setup, we can also access each of these ES modes with the only difference that in our case, there is no imposed flow rate. For our experiments then, the electrode potential is the cuvette surface potential V_S produced through contact electrification, which can be varied by the level of contact, e.g., by the number, type, or intensity of contacts. As a starting case, consider the concentrations $C_{NaOH} = 12.5\,mM$ and $C_{acid} = 1.0\,mM$ originally used by FH, in which case we can produce both the self-sustained oscillations mode and the steady tip-streaming mode of droplet formation. These are analogous to the pulsed cone-jet and cone-jet modes observed in traditional ES experiments, and a comparison of the images shown in Figures 7(a) and 7(b) indicates a remarkable similarity in appearance. For this particular set of concentrations, the equilibrium interfacial tension is fixed at $\sigma_{eq} \sim 3\,mN/m$ (cf. Table II). It proves to be difficult to charge the cuvette sidewall via contact electrification to a value of V_S necessary to produce multicone-jet behavior. However, by increasing the concentration of linoleic acid in the oil phase, the

equilibrium interfacial tension can be lowered to $\sigma_{eq} \sim 0.1\,\mathrm{mN/m}$, which permits a more dramatic multicone-jet mode (not observed by FH as they limited themselves to $C_{acid} = 1.0\,\mathrm{mM}$) to occur for the same levels of V_S produced by contact electrification. On the other hand, by reducing the concentration of linoleic acid, e.g., to $C_{acid} = 0.1\,\mathrm{mM}$ with $\sigma_{eq} \sim 18\,\mathrm{mN/m}$, we can increase the equilibrium interfacial tension, in which case it is difficult to even produce steady tip-streaming behavior with only contact electrification, although self-sustained oscillations (or pulsed cone-jets) are accessible. A more quantitative comparison between the predicted and measured transition to the cone-jet mode will be made in Sec. III, where we found it necessary to develop a new experimental setup with control over the externally imposed electric field strength.

III. THE ROLE OF CHEMICAL REACTION: IS CRDTS A STANDARD ELECTROSPRAY?

Having understood the true origin of CRDTS, the important question left is what is the role of the chemical reaction beyond simply lowering interfacial tension, which makes it possible for the electrospray to be observed for low voltages? Also, because of the presence of surfactant, motion of the interface, and emission of surfactant-laden droplets, is it possible that Marangoni stresses develop along the drop interface and have some influence on the characteristics of the observed ES phenomenon? To address these questions precisely, one needs to use well-controlled externally imposed electric fields instead of not-so-well characterized static electricity discussed in Sec. II B.

To elucidate any role played by surfactant-induced Marangoni stresses, we performed three sets of experiments: (1) quantifying the droplet emission frequency for the pulsed cone-jet mode, which provides information on the timescale of droplet production and the creation of new interface which can be compared to rates of surfactant production via the chemical reaction (Sec. III C), (2) measuring the spray current, droplet size, and frequency in the cone-jet mode (Sec. III D 2) for comparison to the ES theory (Sec. III B 2), and (3) quantifying the flow field in the vicinity of the water-alkali and oil-acid interface during the cone-jet mode (Sec. III D 1), which helps us to estimate the velocity of the interface and then to compare it to the values from the ES theory[53] (Sec. III B 3) and estimates of Marangoni contributions (Sec. III D 3). Altogether, such comparisons allow us to answer the question as to whether CRDTS is a traditional ES or not.

A. Materials and methods

Modifications to the experimental setup were required in order to control the electric field strength in the vicinity of the water-alkali pendant drop, cf. Figure 8. In the new setup, the stainless steel needle immersed in a small container filled with the oil-acid solution is maintained at a potential V using a high-voltage power supply (PS325, Stanford Research Systems) and is positioned a distance H from a grounded planar electrode. This arrangement is typical of ES systems.[49,54,55] To work under the conditions of the original

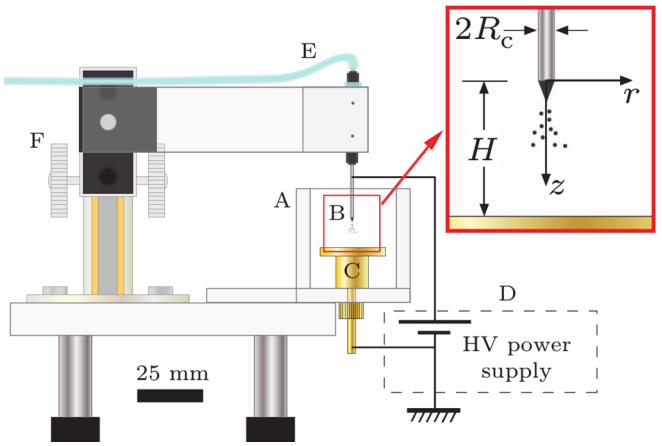

FIG. 8. Experimental setup used to control electric field strength in the vicinity of the capillary tip with components found in a typical electrospray apparatus. The setup includes a non-conducting cell holding the oil-acid mixture (A), a submerged stainless steel needle (B), a circular brass electrode (C), and a high voltage power supply (D) used to maintain a fixed potential between the needle and the bottom electrode. Similar to the setup in Figure 4, the water-alkali solution is supplied to the needle tip using plastic tubing (E) and a syringe pump (not shown). The vertical position of the needle is manipulated by the linear stage (F), setting the distance H between the needle tip and the bottom electrode (see the inset).

CRDTS experiments, we used separation distances of approximately $H \sim 5 - 10\,\mathrm{mm}$ and did not attempt to deliver a constant flow rate Q of water-alkali solution (which is a typical control parameter in standard ES systems). Instead, we began each experiment by forming a water-alkali drop at the tip of the needle. Quantitative information regarding the oil phase flow field was obtained by analyzing the motion of small tracer particles (25 μm polystyrene microspheres, Duke Scientific) using a custom MATLAB program.

Again, all of the experiments were performed using the reagent concentrations listed in Table II. Recall that for these water-alkali oil-acid combinations, only the linoleic acid concentration is varied, while the NaOH concentration is fixed so that the conductivity of the electrosprayed liquid does not change, but the interfacial tension does change dramatically.

Although we varied the voltage V in the course of experiments, we will report results in terms of the electric field strength E at the tip of the needle calculated using

$$E = \frac{V}{0.667\,R_c \ln(4H/R_c)}\,, \tag{2}$$

which is valid for the capillary-planar electrode configuration encountered in many ES setups; here, R_c is the radius of the capillary, H is the capillary-to-plane separation distance (cf. inset of Figure 8), and the constant 0.667 is based on an empirical fit of ES spray data.[55] The rationale for using E, instead of V, in the presentation of the results is to eliminate any dependence of the droplet formation frequency on H/R_c.[56]

B. Expected ES properties

To set the stage before discussing the results of experimental measurements, we outline the key quantitative

properties—transition to the cone-jet mode, electrospray droplet size and current, interfacial velocity—to be expected should our system obey the standard ES theory.[57]

1. Transition to the cone-jet mode

As mentioned in Sec. II B 3, the transitions between many ES modes are not well defined;[48] however, the transition to the cone-jet mode (Taylor cone mode) has been more extensively studied both theoretically and experimentally, e.g., Smith.[55] The electric field strength corresponding to this transition can be adequately predicted using Eq. (3) below, which results from a balance between normal interfacial tension stresses and electrical stresses over the conical interface producing the Taylor cone angle $\theta_{TC} = 49.3^\circ$. For a clean interface, there is only one specific value of σ, which does not change with time, and the transition from the pulsed cone-jet to cone-jet mode should occur when $E = E_{TC}$, where E_{TC} used for non-dimensionalization corresponds to the Taylor cone value

$$E_{TC} = \left[\frac{2\,\sigma \cos\theta_{TC}}{\epsilon_r \epsilon_0 R_c}\right]^{1/2}, \tag{3}$$

which is on the order of 2.0, 1.1, and 0.39 kV/mm for the corresponding acid concentrations $C_{acid} = 0.1$, 1.0, and 10 mM explored in the present study (cf. Table III) and based on the values of $\sigma = \sigma_0$ as will be explained in Sec. III C 2.

2. Electrospray drop size and current

The scalings for droplet size d and electric current I,

$$d/d_0 \sim f_1(\beta)(Q/Q_0)^{1/3}, \tag{4a}$$

$$I/I_0 \sim f_2(\beta)(Q/Q_0)^{1/2}, \tag{4b}$$

have been shown in the literature[52] to compare favorably for a variety of spray liquids (vast range of conductivities and surface tensions) both in an air/gas environment (very typical) and in a liquid environment; the notations used in (4) include $Q_0 = (\sigma\,\epsilon_{r,oil}\epsilon_0)/(\rho\,\kappa)$, $d_0 = [(\sigma(\epsilon_{r,oil}\epsilon_0)^2)/(\rho\,\kappa^2)]^{1/3}$, $I_0 = [(\epsilon_{r,oil}\epsilon_0\sigma^2)/\rho]^{1/2}$, as well as the factors $f_1(\beta) \sim 3$ and $f_2(\beta) \sim 2.5$ for our experimental conditions. For the scalings (4) to apply, it is required that $\delta_\mu \delta^{1/3} \leq 1$, where $\delta_\mu = [(\rho\,\epsilon_{r,oil}\epsilon_0\,\sigma^2)/(\kappa\,\mu^3)]^{1/3}$ is a "viscous parameter" and $\delta = Q_0/Q$ a dimensionless flow rate ratio.

TABLE III. Effective interfacial tension $\sigma_{0,eff}$ used to produce a $E/E_{TC} = 1$ transition in Figure 9(c) as well as the standard k and modified k_s chemical reaction rate constants.

C_{acid} [mM]	σ_{eq} (Ref. 27) [mN/M]	σ_0 (Ref. 27)[a] [mN/M]	$\sigma_{0,eff}$ [mN/M]	k [s^{-1}]	k_s [s^{-1}]
0.1	18	27	30	0.01	1.1
1.0	3	8	12	0.07	1.7
10.0	0.1	1	4	0.02	1.0

[a]These are the largest values of σ corresponding to the start of the dynamic interfacial tension measurements. For the case of the pendant drops used by Touhami *et al.*,[27] these values correspond to $t = 1$ s after the drop formation so they are not for the interface at the ideal $t = 0$.

Using our fluid properties, we find that $\delta_\mu \sim 0.2$ and $\delta \sim 3 \times 10^{-4} - 3 \times 10^{-3}$ for the measured flow rates $Q = 0.3 - 2.5$ nl/s (cf. Sec. III D 2), so that indeed $\delta_\mu \delta^{1/3} \sim 0.01 - 0.03 \leq 1$. This allows us to use (4 a) to predict the droplet size. For our conditions, $Q_0 = 7.8 \times 10^{-16}\,m^3/s$ and $d_0 = 3.7 \times 10^{-9}$ m. Putting this all together, if we had a true electrospray, we would expect that the droplet size would be approximately $d \sim 0.08 - 0.2\,\mu$m. Note that such a small droplet size is typical of highly conducting liquids. As a comparison, consider the data of Smith[55] who added NaCl to water to bring the conductivity up to ~0.5 S/m—roughly the same as our conductivity—and reported droplets with diameters less than ~0.1 μm. Also, we can predict the current based on (4 b), where for our conditions, $Q_0 = 7.8 \times 10^{-16}\,m^3/s$ and $I_0 = 1.7 \times 10^{-9}$ A, so that we would expect the spray current to be approximately $I \sim 8.3 \times 10^{-8} - 2.4 \times 10^{-7}$ A if we had a true electrospray.

3. Interfacial velocity

To answer the question if the observed magnitude of $U_{S,meas}$ (cf. Sec. III D 1) hints at a role played by Marangoni stresses at the interface, we need to estimate the magnitude of $U_{S,ES}$ if we consider only the ES contribution. As presented by Barrero *et al.*[53] for modeling flows inside Taylor cones, $U_{S,ES}$ can be determined from a balance between tangential electrical stresses and viscous stresses at the interface.[58,95,96] Given the much larger viscosity of the oil in our liquid-liquid experiments, we shall neglect the viscous stresses from the water phase. The tangential stress balance at the interface is then

$$\epsilon_{r,oil}\epsilon_0 E_\tau E_n \sim \mu_{oil} U_{S,ES}/L, \tag{5}$$

where E_τ is the tangential component of the electric field (which varies with position along the interface) and L a characteristic dimension over which the velocity in the oil phase varies by $\sim U_{S,ES}$. We will take $L \sim R_c$ and the normal component of the electric field as given by Eq. (3). The tangential component of the electric field along the interface will vary as $E_\tau \sim I/(\kappa r^2)$, which essentially comes from Ohm's law with I/r^2 being the current density and κ the conductivity. As we seek to estimate the value of $U_{S,ES}$ averaged over the interface, we will again choose $r \sim R_c$ for the tangential electric field. After substitution, we arrive at the following order of magnitude estimate of the interface velocity:

$$U_{S,ES} \sim \left(\frac{\sigma\,\epsilon_{r,oil}\,\epsilon_0 I^2}{R_c^3\,\kappa_{NaOH}^2\,\mu_{oil}^2}\right)^{1/2}. \tag{6}$$

Using the droplet size and emission frequency corresponding to the flow rate range mentioned previously in Sec. III B 2 (i.e., $Q = 0.3$–2.5 nl/s), and estimating the current based on the Rayleigh charge limit (maximum limit of charge on a drop), $I = I_R$, we find that $U_{S,ES} \sim 1.6 - 3.2 \times 10^{-7}$ mm/s.

C. Modes and transitions: CRDTS vs electrosprays

From the observations of CRDTS phenomena, we have learned that we can produce different modes of droplet

emission (Sec. II B 3) by varying the potential V (or equivalently E). For each of the linoleic acid concentrations listed in Table II, we measured the droplet emission frequency f, which in the pulsed cone-jet mode (SSO) is chosen to correspond to the drop oscillation frequency and in the cone-jet (ST) mode to the true frequency of formation of individual droplets, as well as the values of E corresponding to the transition between pulsed cone-jet and cone-jet modes. The results from these experiments are shown in Figure 9(a).

It is apparent from Figure 9(a) that with decrease of acid concentration (and thus increase of σ_{eq}), the magnitude of E corresponding to a transition between different modes increases. For each of the acid concentrations, the frequency f increases with E until transition to the cone-jet mode occurs. At low values of E, only drop deformation, without droplet emission, is observed (black markers). This is followed by a transition to the pulsed cone-jet mode with relatively low droplet emission frequency f (gray markers). Increasing E within the pulsed cone-jet mode increases f until an abrupt transition to the steady cone-jet mode occurs where $f \gg 100\,\mathrm{s}^{-1}$ (white markers). This sequence of modes is qualitatively analogous to that portrayed in Figure 7(a), where V_S is varied by the level of static charge on the cuvette sidewall. While in our case, there is no imposed flow rate, such a sequence is typical of ES systems with fixed flow rates. Each data point is obtained by starting with a new drop at the tip of the capillary and stepping the potential V to the desired value.

Given our new understanding that the oscillation frequency changes with E as well as with C_{acid} (in other words with σ_{eq} and chemical reaction rate k), we can perform quantitative comparison with the ES theory. While the pulsed cone-jet mode in traditional ES systems does not have a well-established theory, we can do quantitative comparison of the measured transition from pulsed cone-jet to cone-jet modes in our system. Therefore, the plan of the present section is to develop a simplified model (Sec. III C 1) to account for the observed oscillation period as well as the mode transition. This will help us to identify the appropriate interfacial tension values (Sec. III C 2), which will play an important role in clarifying the role of Marangoni effects (Sec. III C 3) and when comparing measurements and standard ES theory for the cone-jet mode in Sec. III D.

1. Model

In the original CRDTS work of FH,[15] a lingering question was what exactly determines the period of drop oscillation. The companion paper by KH[19] addressed this question using a relaxation oscillator model—a mechanical model of the dynamics of the pendant drop.[59] In that model, the interfacial tension changes with time due to formation of surfactant as the result of the chemical reaction (described by a reaction rate k), and the results of the model demonstrated that reaction rate can dictate the oscillation frequency. However, the trends presented in Figure 9(a) can be produced from an even simpler model as discussed below.

Considering the balance of the azimuthal capillary stress and the Maxwell normal stress at the fluid-fluid interface,[44,54] the pressure drop across a curved interface of radius R is

$$\Delta p = \frac{2\sigma}{R} - \frac{1}{2}\epsilon_r \epsilon_0 E_n^2, \tag{7}$$

where σ is the interfacial tension (assumed here to be uniform along the interface), ϵ_r is the relative permittivity of the

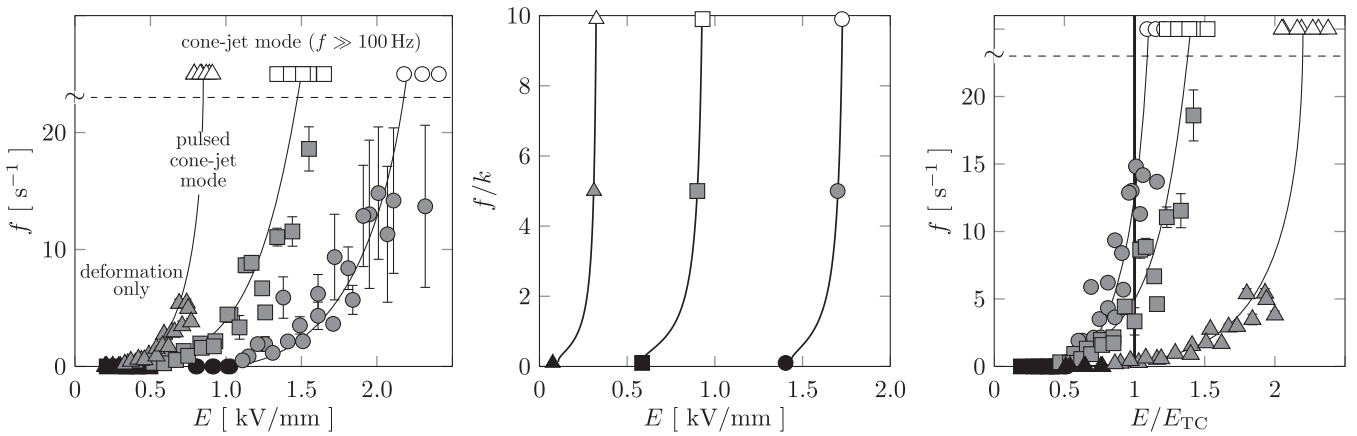

(a) drop formation frequency and modes. (b) simple model for $f(E)$. (c) E normalized by cone-jet onset E_{TC}.

FIG. 9. Measurements of droplet emission frequency using the CRDTS chemistry and the ES setup, cf. Figure 8. In all experiments, $C_{NaOH} = 12.5$ mM was held fixed but the linoleic acid concentration was varied: $C_{acid} = 0.1$ mM (○), $C_{acid} = 1.0$ mM (□), and $C_{acid} = 10.0$ mM (△). Black markers denote conditions where the electric field E only causes deformation of the interface (no droplet emission), gray markers denote the pulsed cone-jet mode, and white markers indicate the cone-jet mode (the cone-jet mode markers only indicate the mode and *not* the actual frequency of drop emission). (a) For each of the reagent combinations, increase in the electric field strength E causes the transition between modes as discussed in Sec. II B 3 (i.e., deformation only → pulsed cone-jet → cone-jet); solid curves are given to guide the eye. Values of E corresponding to the mode transitions increase with decreasing C_{acid}. (b) The model (10), that considers a balance between time dependent interfacial tension and electrical forces, can qualitatively predict the behavior shown in (a). Markers have been included on each of the lines to differentiate between the values of C_{acid}. (c) Normalizing the data from (a) by the theoretical value of E_{TC} corresponding to the onset of the cone-jet mode given by Eq. (3) suggests that increased surfactant production (with C_{acid}) shifts the mode transition E to values higher than predicted. *Note* that in (b) and (c), we intentionally departed from the standard convention to plot dimensional vs. dimensional (or non-dimensional vs. non-dimensional) variables to avoid crowding the data.

ambient fluid, and E_n is the normal component of the electric field at the interface. If we think of the interface as rupturing when $\Delta p = 0$, this occurs when (dropping all numerical constants),

$$\frac{\sigma}{R} \sim \epsilon_r \epsilon_0 E_n^2, \tag{8}$$

i.e., when $\sigma(t)$ reaches some critical value (for a fixed E_n) for a system with surfactant production. For our water-alkali oil-acid system, the interfacial tension decreases with time t and is usually described by first-order reaction kinetics[26,60] as

$$\sigma(t) = \sigma_{eq} + (\sigma_0 - \sigma_{eq})e^{-kt}, \tag{9}$$

where k is the reaction rate constant, σ_0 is the initial interfacial tension (at $t = 0$), which for the case of acidified oils may be acid concentration dependent,[27] and σ_{eq} is the equilibrium interfacial tension (at $t \to \infty$), which may not be achieved in practice for a system in which new interface is being created. For the interface of the water-alkali drop in the presence of the chemical reaction, $\sigma(t)$ will eventually decrease to a critical value at time t_{crit}, at which the interface ruptures for a given applied field E. After the interface ruptures, i.e., emits droplets, the interfacial tension relaxes back to σ_0 and the process repeats. Using this reasoning and Eqs. (8) and (9), the frequency of droplet emission $f \sim t_{crit}^{-1}$ scales as

$$\frac{f}{k} \sim \left[\ln \frac{\sigma_0 - \sigma_{eq}}{\epsilon_{r,oil}\epsilon_0 R E_n^2 - \sigma_{eq}}\right]^{-1}, \tag{10}$$

which is valid only for a particular range of electric field strength $E_{n,min} = \sqrt{\sigma_{eq}/(\epsilon_{r,oil}\epsilon_0 R)} \lesssim E_n \lesssim E_{n,max} = \sqrt{\sigma_0/(\epsilon_{r,oil}\epsilon_0 R)}$. Using the corresponding values of interfacial tension in Table III and $R = R_c$, it is convenient to plot the ratio f/k from Eq. (10) for each of the acid concentrations—these are shown as the solid lines in Figure 9(b). A favorable qualitative comparison exists between the experimental data of Figure 9(a) and the simple model (10) leading to Figure 9(b). The drop deformation only to the pulsed cone-jet mode transition is analogous to the lower limit $E_{n,min}$. The droplet emission frequency f increases with E_n, and the rapid increase in f near $E_{n,max}$ for the model is similar to the pulsed cone-jet to the cone-jet transition of the data. The model even shows the shift in curves with changes in acid concentration, manifested as differences in k, σ_{eq}, and σ_0. However, if one relies on $\sigma(t)$ data collected from pendant drop experiments with no fluid motion, the model (10) fails to quantitatively predict the experimentally measured magnitude of f. This is because, unlike for the conditions in our experiments, the available data[27] fail to capture details of $\sigma(t)$ for interface ages less than 1 s—this fact is important given the frequency of oscillations encountered in our experiments. We note that larger values of k will result if reliable data for $\sigma(t < 1\,\text{s})$ can be obtained. Indeed, if one uses the values of $k = k_s$ estimated for short times $t < 1$ s, cf. Appendix B and Table III, then the model (10) gives the right order of magnitude of the frequency, cf. Figure 17(c) in Appendix B.

2. Transition to the cone-jet mode

If we normalize the data shown in Figure 9(a) by E_{TC} given by (3), calculated using the value σ_0, we can observe the following, cf. Figure 9(c). With increasing concentration of linoleic acid, corresponding to an increase in the amount of surfactant produced at the interface, the transition between the pulsed cone-jet and cone-jet modes shifts to larger values of E/E_{TC}. In order to bring the transition value of E/E_{TC} from the intermittent cone-jet to the cone-jet mode to $E/E_{TC} = 1$, an effective interfacial tension $\sigma_{0,eff}$ should be used in Eq. (3) instead of σ_0, which meaning will be clarified in the discussion below and which values are provided in Table III. It must be pointed out that $\sigma_{0,eff}$ exceeds the initial (in time) value σ_0 that is often reported for the oil-water interface with these chemicals.[27] This may, at first, seem unphysical but the values of σ_0 are based on traditional pendant drop measurements that cannot be used for short (less than 1 s) time measurements of dynamic interfacial tension, while in our case, we need the short-time values of σ_0 as droplets are formed with a frequency greater than 1 Hz. To get a sense of these values, referred to here as $\sigma_{0,eff}$ (since in the model (10), we neglect any effects of variation of the interfacial tension along the interface), one can use the following argument. The data of Touhami *et al.*[27] suggest that linoleic acid itself is somewhat surface active—the authors[27] also report measurements of the dynamic interfacial tension of a water-acidified oil interface (Figure 1 of their work). So even without the addition of sodium hydroxide, the interfacial tension of the acidified oil-water interface can change with time. The approximate values of interfacial tension of the acidified oil-water interface (without the alkali in the water phase) for the reagents tested are given in Table IV, where $\sigma_{0,a}$ is the initial value and $\sigma_{eq,a}$ is the equilibrium value (note that there is no surfactant generation at the interface). In our droplet formation experiments, the interface is being rapidly depleted of surfactant, but there is always the presence of the weakly surface active linoleic acid. As a result, the effective initial interfacial tension $\sigma_{0,eff}$ for the NaOH-linoleic acid systems listed in Table III must fall somewhere above the initial value for the surfactant interface (referring to σ_0) and below the equilibrium value of the linoleic acid only interface (from Table IV). In other words, we expect $\sigma_{0,a} > \sigma_{0,eff} > \sigma_0$ based upon the differences in the interfacial tensions of acidified oil-water interfaces (with no surfactant present, only weakly surface active acid) and acidified oil-water alkali interfaces (with highly surface active surfactants formed as a result of the chemical reaction between acid and alkali). Note that the values of $\sigma_{0,eff}$ determined from the data of Figure 9(c) are not presented in the

TABLE IV. Measurements of the dynamic interfacial tension of a water-acidified oil interface[27] (without the alkali in the water phase).

C_{acid} [mM]	$\sigma_{0,a}$ [mN/M]	$\sigma_{eq,a}$ [mN/M]
0.1	52	45
1.0	45	31
10.0	30	19

literature[27] in plots of dynamic interfacial tension, $\sigma(t)$, because they would correspond to values of time inaccessible in a basic pendant drop apparatus (i.e., less than 1 s).

In summary, the simple model (10) for the drop emission frequency can qualitatively predict the $f(E, C_{\text{acid}})$ trend observed in experiments. However, the magnitude of f predicted from Figure 9(b) using the standard values of the chemical rate constant k, cf. Table III, is too low compared to the frequencies measured in experiments, cf. Figure 9(a). As discussed in Sec. III C 1, better quantitative agreement is achieved if one uses the modified values of the reaction rate k_s estimated from the short-time data of Touhami *et al.*[27] (cf. Appendix B), especially for low droplet emission frequencies in the pulsed cone-jet mode, cf. Figure 17(c) in Appendix B.

3. Implications for Marangoni effects

Returning to the main purpose of Sec. III, do the data presented in Figure 9 suggest any influence of Marangoni effects? There are three pieces of evidence that point toward a *possible* influence. First, there is a shift in E/E_{TC} corresponding to the transition from the pulsed cone-jet to the cone-jet mode, which has not been previously reported in the literature for systems without surfactant[55] (a discussion in the context of other electrospray systems with surfactants will be given in Sec. III E). Furthermore, the magnitude of the shift increases with acid concentration C_{acid}, which corresponds to the decrease in σ_{eq}, cf. Table III. As Marangoni stresses are proportional to $\Delta\sigma = \sigma_{0,\text{eff}} - \sigma_{\text{eq}}$, a reduction in σ_{eq} will lead to an increase in $\Delta\sigma$ and thus the observed shift in E/E_{TC} may in fact be due to Marangoni effects. Second, there is a difference in the drop emission frequencies f obtained by Eq. (10) and those measured in experiments for the pulsed cone-jet mode. The model (10), which considers only a uniform decrease in interfacial tension resulting from the chemical reaction, fails to account for any accumulation of surfactant at the tip as a result of interfacial motion. It is possible then that Marangoni stresses can give rise to interfacial motion that sweeps surfactant to the tip faster than it is produced by the chemical reaction, thus enhancing the drop emission frequency calculated from Eq. (10). Third, the upper values of Damkohler numbers in the range $Da = k_s/f \sim 0.001 - 1$ corresponding to our experiments suggest that surfactant concentration gradients may exist along the interface. Here, the droplet production frequency f is measured in the pulsed cone-jet mode for the experiments, cf. Figure 9(a).

D. Interfacial processes and droplet emission

While we know that (a) droplet formation occurs only as a result of application of an electric field, (b) increasing the electric field intensity shows that we can produce several modes of droplet production (dripping, cone-jet, multicone-jet), and (c) the transition to the cone-jet mode is in the neighborhood of E_{TC} corresponding to the formation of a Taylor cone, the question is whether or not we actually observe *a traditional electrospray*. Addressing this requires more detailed observations, in particular to see (1) if the droplet sizes and spray electric currents follow the scaling laws for the ES theory[57] and (2) what is the origin of the interfacial convective velocity $U_{\text{S,meas}}$, which is driven by both the tangential component of electric stresses $E_\tau \neq 0$ and Marangoni stresses. For such a comparison, we need measurements of droplet size, spray current, and interfacial velocity in the "cone-jet" mode.

1. Measurements of the flow near the interface and droplet motion

There are only a limited number of experimental reports of flow visualization for ES systems,[53,61] and, to the authors knowledge, all of these instances—typically, the flow field in the sprayed liquid—are for liquids sprayed into gases. Thus, our goal is to quantify the flow field in the external phase near the needle tip in order to estimate the interface velocity U_S.

An ES experiment was performed using the setup shown in Figure 8 with $C_{\text{NaOH}} = 12.5\,\text{mM}$ and $C_{\text{acid}} = 1.0\,\text{mM}$ solutions. The potential $V = 2000\,\text{V}$ was selected to correspond to the cone-jet mode as this mode has been extensively studied in the ES literature. Small tracer particles were added to the oil phase in order to measure the flow field in the vicinity of the interface. Although the cone-jet mode produces a large number of droplets that can be used as tracers, their trajectory is expected to be influenced by their charge. The motion of the tracer particles, analyzed using a MATLAB code, is shown in Figure 10 along with corresponding streak images (formed by an overlay of 500 high speed movie frames). The origin of the rz coordinate system is indicated in the inset of Figure 8. The recorded motion is in a plane defined by the shallow depth of focus of the camera/lens system.

a. Large scale motion. Consider first the large scale motion that is readily observed in Figure 10(a). The circulation is the inevitable result of the close proximity of the large planar electrode at the bottom of the cell, cf. Figure 8. Charged droplets are ejected from the tip of the oil-water interface and continue to move in the z direction and propelled toward the planar electrode entraining oil with them, as in any spray. The droplets tend to follow trajectories that appear similar to the electric field lines emanating from the capillary and terminating at the planar electrode, cf. Appendix C1.

b. Droplet and interface velocities. Next, consider the flow field close to the oil-water interface presented in Figure 10(b). A detailed look reveals that the velocity of the droplets U_d decays from $\sim 22\,\text{mm/s}$ at $z = 0.5\,\text{mm}$ (near the tip of the interface) to $\sim 10\,\text{mm/s}$ at $z = 2\,\text{mm}$ and to $\sim 7.5\,\text{mm/s}$ at $z = 3\,\text{mm}$. So the axial velocity of the droplets decreases with distance from the tip of the interface/needle. The average radial velocity in the region near $z = 0.5\,\text{mm}$ (and near the axis as can be seen in the flow field image) is on the order of $\sim 5\,\text{mm/s}$, but it is also observed that many droplets have little or no radial motion. The "spray cone" angle appears to be in the range of $\sim 60^\circ - 80^\circ$, similar to that reported in KH based on the images of FH; details of the spray structure are discussed in Appendix C2.

The best estimate that we can make of the interface velocity is $U_{\text{S,meas}} \sim 3\,\text{mm/s}$ with the standard deviation

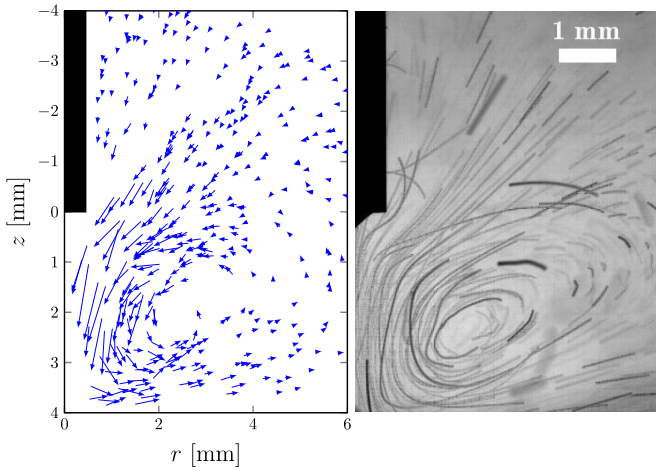

(a) Large scale fluid motion (500 frame overlay – 200 fps).

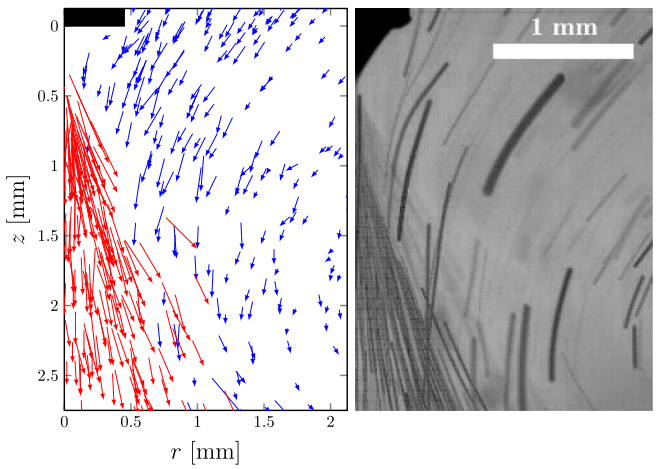

(b) Flow field near needle tip (500 frame overlay – 4000 fps).

FIG. 10. Streakline images and corresponding velocity vector fields for the conditions of $C_{acid} = 1.0\,mM$, $C_{NaOH} = 12.5\,mM$, $h/r_c = 10$, and $V = 2000\,V$ (or $E/E_{TC} = 2.7$). Notice that in (b), the motion of the outer phase (oil) is affected by the droplet emission even several mm from the capillary tip. Closer inspection of the flow field near the tip of the capillary (a) indicates a velocity of the oil phase on the order of $\sim 3\,mm/s$, while the ejected droplets (red) have axial velocities on the order of $\sim 10 - 20\,mm/s$.

0.9 mm/s, based on the average tracer particle velocity in the region bound by $0 < z < 0.5\,mm$ and $0 < r < 1\,mm$. Also, from our velocity field measurements, we can calculate two values of the Reynolds number, $Re_d = \rho_{oil} U_d d/\mu_{oil} = O(10^{-3})$ based on the observed droplet diameter range $d = 6 - 20\,\mu m$ and speed, and $Re_{R_c} = \rho_{oil} U_d (2R_c)/\mu_{oil} = 1 \times 10^{-2}$ based on the oil phase velocity and the needle diameter $2R_c$: thus we operate in the Stokes regime.

The measured value $U_{S,meas}$ should be contrasted with the value expected from the ES theory (Sec. III B 3), which is $O(10^{-6}\,mm/s)$. This exceptionally low value is associated with the high conductivity of the sprayed liquid, suggesting very small electrical shear stresses on a major part of the interface. Near the apex of the cone-shaped interface, these stresses will increase with the distance r as $E_\tau \propto 1/r^2$; however, the dimension at which they would produce surface velocities on the order of those observed, i.e., $U \sim 1\,mm/s$, are incompatible with our experiments. For example, the value of r corresponding to R_c in Eq. (6), at which it yields $U_{S,ES} = 1\,mm/s$, would be about $3\,\mu m$. This is well below even the size of the observed droplets. This substantial discrepancy between $U_{S,meas}$ and $U_{S,ES}$ will be revisited in Sec. III D 3 in the context of the discussion of Marangoni effects.

2. Electric field effects

First note that the charge relaxation timescale is given by $\tau_e \sim \beta\epsilon_0/\kappa \sim 10^{-9}\,s$, where $\beta = \epsilon_{r,NaOH}/\epsilon_{r,oil}$, which is a very fast timescale owing to the high conductivity of the sodium hydroxide solution, i.e., sprayed (inner) liquid, the concentration of which was fixed for all experiments. Since τ_e is much faster than the hydrodynamic timescale, the use of the electrospray equations based on electrostatics is justified.

a. Droplet size and emission frequency. We extracted drop size from the high-speed movies for "cone-jet" conditions for $V = 2000\,V$, a needle-to-plate separation distance of approximately ten needle radii, and the reagent concentrations from the original CRDTS experiments ($C_{NaOH} = 12.5\,mM$ and $C_{acid} = 1.0\,mM$). As one can observe from Figure 11, initially the droplets are large ($d > 20\,\mu m$) and form with a frequency near $f \sim 1000\,s^{-1}$, which corresponds to a flow rate of $Q \sim 2.5\,nl/s$. With time, the droplet size decreases and the droplet frequency increases until at later times, e.g., $t = 200\,s$, the droplets have an approximate diameter of $d \sim 6\,\mu m$ (Ref. 62) and are formed at $f \sim 3000\,s^{-1}$, so that the flow rate $Q = f_d\,\pi\,d^3/6 \sim 0.3\,nl/s$. Given the range of values of Q, we can estimate the hydrodynamic timescale $\tau_h \sim LR^2/Q = O(10^{-3}\,s)$, where $L \sim 10R$ and $R \sim 20\,\mu m$ are the characteristics length and radius of the spray jet.

b. Electrospray current. As suggested by Figure 12, when the electric field is applied at $t = 0\,s$, the initially hemispherical drop is pulled into a cone shape. Large droplets are produced ($d > 20\,\mu m$) and carry a current of $I \sim 1\,nA$. Very quickly, the drop volume is reduced, the emitted droplets shrink in size with a corresponding increase in droplet

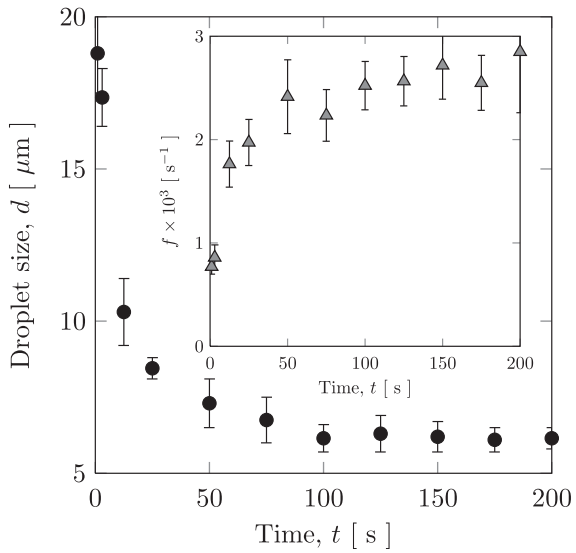

FIG. 11. Measured droplet diameter d and emission frequency f under the conditions of $V = 2000\,V$ and $H/R_c \sim 10$.

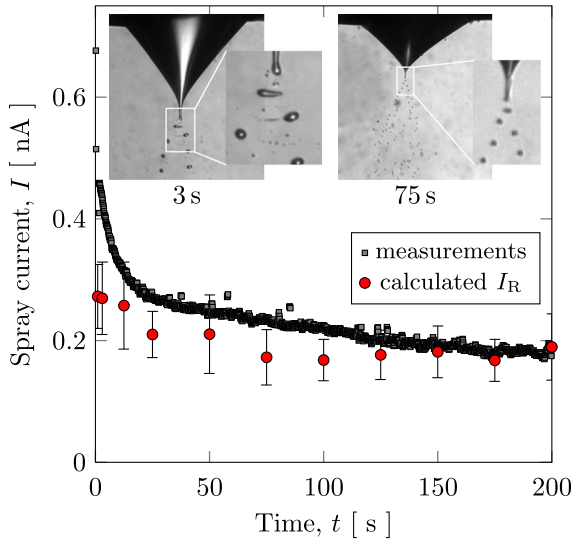

FIG. 12. Measurements of the spray current I for $V = 2000\,\mathrm{V}$ and $H/R_c \sim 10$ with a Keithley 6485 picoammeter.

formation frequency ($>1000\,\mathrm{s}^{-1}$), and the current decreases as well.

We can estimate the maximum allowable spray current I_R (circles) over the course of the experiment using the droplet size, emission frequency, and the Rayleigh charge limit, $q_R = 8\pi(\epsilon_{r,oil}\,\epsilon_0\,\sigma\,r^3)^{1/2} = O(10^{-12}\,\mathrm{C})$, where r is the droplet radius, $\epsilon_{r,oil}$ the permittivity of oil, and the interfacial tension is taken as $\sigma = \sigma_{0,eff} = 12\,\mathrm{mN/m}$ from Table III. We find that early in the electrospraying process $I > I_R$ suggesting the emitted droplets should break apart owing to the unstable level of charge. This is in fact what is observed (see the 3 s image inset in Figure 12). At later times, the spray current is $I \lesssim I_R$ suggesting that the emitted droplets should be stable.

c. Comparison. Let us now make some comparisons with the values expected from the ES theory (Sec. III B 2). First, our observed values of drop diameter are $d \sim 6 - 20\,\mu\mathrm{m}$; however, the estimates from the electrospray equations suggest $d \sim 0.08 - 0.2\,\mu\mathrm{m}$! There is approximately a factor of $O(10^2)$ discrepancy between the two values. Also note that we can deduce the electrospray droplet production frequency f from the values of Q and d. The result is that if the droplets were $d \sim 0.08 - 0.2\,\mu\mathrm{m}$ in size, they would be produced at a rate of $f \sim 10^9$ drops/s! This characteristic of standard ES is well in excess of our observed value of $\sim$1000 drops/s. This immediately points to a discrepancy between the traditional electrosprays discussed in the literature (lower conductivity, liquid-in-air) and our liquid-in-liquid "electrospray," with low interfacial tension and an insoluble surfactant present.

Another difference worth pointing out is the variation of droplet size with voltage in the cone-jet mode—for example, compare the droplet diameter in the cone-jet mode corresponding to the flow visualization experiments and the nearly imperceptible droplets formed in the ST mode shown in Figure 7—this observation is also in disagreement with typical ESs, which do not exhibit a strong variation in droplet size with voltage in the cone-jet mode.

Finally, we can consider the spray current. Recall that we are interested in the transient spray as it is similar in nature to the CRDTS phenomenon reported by FH whereas typical electrosprays are analyzed for steady conditions (with an imposed flow rate). Yet, even for later times when the decay of I with time is small, measured currents are well below those predicted by the electrospray equations based on the liquid properties and estimated flow rates (from measured droplet size and frequency), i.e., for the conditions shown in Figure 12 ($Q/Q_0 \sim 400$), we find that our measured spray current $I/I_0 \sim 0.1$ whereas other liquid-liquid electrosprays[52] for nearly the same Q/Q_0 have been reported to scale well with the electrospray equations, which result in a calculated value of $I/I_0 \sim 100$.

d. Summary. Although the observed droplet formation process shares many attributes with electrospraying, a simple analysis based on a few observations suggests that the mechanisms dictating droplet size and spray current in our setup are not the same as for standard ES. What we observe is not a traditional electrospray. This difference is likely the result of the insoluble surfactant generated at the interface along with associated Marangoni stresses and the viscosity ratio of the liquid-liquid combination. While the latter will be discussed in Sec. III E, the former will be addressed in Sec. III D 3.

3. Marangoni effects

To estimate the interfacial velocities driven solely by surfactant concentration gradients, let us ignore the imposed electric field and suppose that Marangoni stresses are balanced by viscous stresses in the external (oil) phase. For simplicity, we shall consider that the velocity $U_{S,M}$ does not vary considerably with position along the interface and that the interfacial tension gradient $\Delta\sigma$ exists along the interface from the base of the drop to the conical tip (a distance of $L \sim R_c$), thus leading to the simple balance

$$\frac{\Delta\sigma}{R_c} \sim \mu_{oil}\frac{U_{S,M}}{L} \quad \text{or} \quad U_{S,M} \sim \frac{\Delta\sigma}{\mu_{oil}}\frac{L}{R_c}, \tag{11}$$

from which we arrive at $U_{S,M} \sim \Delta\sigma/\mu_{oil}$.

In order to estimate $U_{S,M}$, we need to choose an appropriate value of $\Delta\sigma = \sigma - \sigma_{tip}$, which ought to be a value that best represents the variation of interfacial tension along the interface. Recall that surfactant would be driven to the tip of the drop by the interface motion and can be crowded well beyond the equilibrium surfactant concentration corresponding to the static conditions between the bulk and interface,[63] so $\sigma_{tip} < \sigma_{eq} = 3\,\mathrm{mN/m}$. Because of the uncertainty in knowing the exact concentration at the tip due interface motion and crowding, we conservatively consider a range of possible values, $0.1 < \sigma_{tip} < 3\,\mathrm{mN/m}$, while we can treat σ as $\sigma_{0,eff}$ in $\Delta\sigma$. Therefore, for the same reagent concentrations as used for the flow field imaging, from which we obtained the measured magnitude of the surface velocity $U_{S,meas}$, we arrive at the estimate $U_{S,M} \sim 41 - 54\,\mathrm{mm/s}$. These large magnitudes of interfacial velocity $U_{S,M}$, compared to the low $U_{S,ES}$ predicted by the electrospray equations, suggest that Marangoni effects should play a role in the observed phenomena.

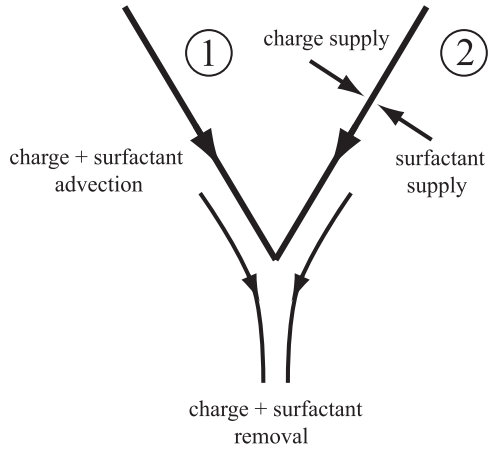

FIG. 13. Key processes of charge and surfactant transport.

Given the above understanding of the electric field and Marangoni effects, we can recapitulate on the overall physics of the CRDTS phenomena, cf. Figure 13. The key processes are (1) charge is transferred from the bulk of the water-alkali phase to the water-oil interface via conduction current at the characteristic time $\tau_e \simeq 10^{-9}$ s; (2) both surface and conduction currents remove charge from the water-alkali phase to the oil-acid phase in the form of droplets at the characteristic time scale $\tau_h \simeq 10^{-3}$ s; (3) surfactant is produced at the chemical reaction rate k_s, i.e., on the time scale not slower than 1 s; and (4) surfactant is removed with the droplets on the time scale $\tau_h \simeq 10^{-3}$ s. Thus, despite that charge supply to the interface is much faster than the surfactant production, since both charge and surfactant are bound to be removed on the same time scale τ_h due to droplet emission, the Marangoni contribution to U_S should be dominant.

From our experiments, using the ES setup of Figure 8, we found that the observed droplet formation in both the pulsed cone-jet and cone-jet modes (analogous to the self-sustained oscillations and steady tip-streaming modes of FH) is influenced by surfactant-induced Marangoni stresses. The electric field strength corresponding to the onset of the cone-jet mode, as compared to the theoretical value, appears to vary with the reagent concentrations (and hence with the interfacial tension). The simple model (10) for the droplet emission frequency qualitatively predicts the $f(E)$ trend observed in experiments, cf. Figure 9, but demonstrates quantitative agreement only for low emission frequencies, which is consistent with the fact that the model does not account for variations in interfacial tension at the tip of the drop. And the Damkohler numbers corresponding to our experiments in the pulsed cone-jet mode are sufficiently low, so that interfacial tension gradients may be present. Furthermore, our estimate of the interface velocity from flow field measurements in the cone-jet mode compare more favorably with scaling based on a balance between Marangoni and viscous stresses than with a balance between electrical shear and viscous stresses, i.e., $U_{S,ES} \ll U_{S,meas} \ll U_{S,M}$. These observations along with previously discussed differences from the standard ES theory summarized in Table V indicate that the surfactant-induced Marangoni stresses have a major effect on the tip-streaming. However, at least in the used combination of chemicals, they cannot lead to the self-sustained CRDTS, the exact mechanism for which, as was pointed out by Stocker and Bush,[64] "*remains elusive*."

E. Further differences from electrosprays

Finally, it is worth mentioning here some key differences in fluid properties between our experiments and electrosprays reported in the literature:

a. Viscosity ratio. In traditional electrosprays, a liquid is sprayed into air and thus the viscosity ratio μ_i/μ_o is much greater than 1 (where i and o stand for inner and outer, respectively), e.g., for water in air it is $\mu_i/\mu_o \sim 50$. However, in our experiments, the viscosity ratio (water in paraffin oil) is $\mu_i/\mu_o \sim 0.005$. Furthermore, the very few instances of liquid-liquid electrosprays in the literature have liquid-liquid combinations with a viscosity ratio greater than 1. For example, in the extensive work by Barrero *et al.*,[52] the lowest viscosity ratio tested is for water sprayed into heptane ($\mu_i/\mu_o \sim 2.5$), so it is perhaps not surprising that these liquid-liquid systems behave similar to liquid-gas electrosprays. Aside from papers on microfluidic flow focusers (imposed flow field) enhanced by electric fields,[65] our system has a unique viscosity ratio compared to electrosprays reported in the literature.

b. Conductivity. Our sprayed liquid conductivity is $\kappa = 0.3\,\mathrm{S/m}$, which is much higher than in traditional electrosprays, cf. Figure 14(a). There are only a handful of published results for liquids with $\kappa > 0.1\,\mathrm{S/m}$, which are primarily water-in-air systems where water is doped with an electrolyte.

c. Surface tension. The interfacial tension of our system is very low—in the range of $0.1 - 20\,\mathrm{mN/m}$. A review of the literature for liquid-air sprays that possess conductivities close to $\kappa \sim 0.1\,\mathrm{S/m}$ suggests that there are no studied systems with a comparable interfacial tension, cf. Figure 14(b). The systems of similar conductivity have surface tensions in

TABLE V. Summary on the differences between CRDTS measurements in the cone-jet mode (for $V = 2000$ V with $C_{NaOH} = 12.5$ mM and $C_{acid} = 1.0$ mM) and estimates based on traditional ES (Sec. III B) and Marangoni scalings (Sec. III D 3). Estimates for $U_{S,M}$, f_M, and I_M are based on $\Delta\sigma = \sigma_{max} - \sigma_{min}$, where $\sigma_{max} = \sigma_{0,eff}$ and $\sigma_{min} \sim 0.1 - 3\,\mathrm{mN/m}$, cf. Sec. III D 3; estimates of d_M follow from Eq. (1).

Measured values	ES estimate	Marangoni estimate	Conclusion
$U_{S,meas} \sim 3\,\mathrm{mm/s}$	$U_{S,ES} \sim 10^{-6}\,\mathrm{mm/s}$	$U_{S,M} \sim 41 - 54\,\mathrm{mm/s}$	$U_{S,ES} \ll U_{S,meas} \ll U_{S,M}$
$d_{meas} \sim 6 - 20\,\mu\mathrm{m}$	$d_{ES} \sim 0.08 - 0.2\,\mu\mathrm{m}$	$d_M \sim 6 - 180\,\mu\mathrm{m}$	$d_{ES} \ll d_{meas} \leq d_M$
$f_{meas} \sim 10^3 - 3 \times 10^3\,\mathrm{drops/s}$	$f_{ES} \sim 10^8 - 10^9\,\mathrm{drops/s}$	$f_M \sim 10^{-1} - 2 \times 10^4\,\mathrm{drops/s}$	$f_M \sim f_{meas} \ll f_{ES}$
$I_{meas} \sim 0.2 - 1.0\,\mathrm{nA}$	$I_{ES} \sim 83 - 240\,\mathrm{nA}$	$I_M \sim 5 \times 10^{-4} - 0.1\,\mathrm{nA}$	$I_M \leq I_{meas} \ll I_{ES}$

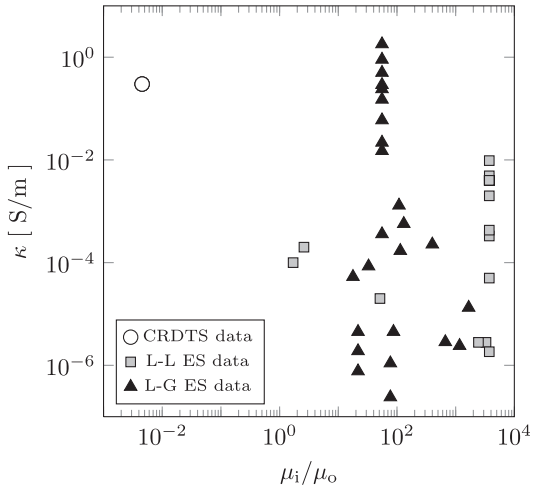

(a) Conductivity κ vs. viscosity ratio μ_i/μ_o.

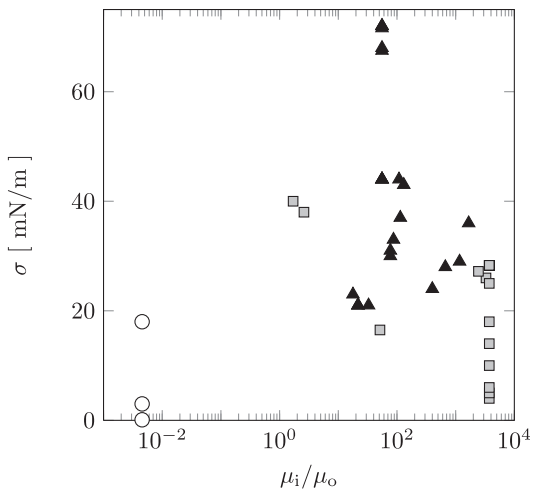

(b) Surface tension σ vs. viscosity ratio μ_i/μ_o.

FIG. 14. Fluid properties of CRDTS versus that of liquid-liquid[52,68,69] (L-L ES) and liquid-gas[55,57,70] electrosprays (L-G ES).

the 50–70 mN/m range, because of the use of water. Liquids such as ethanol, hexane, and heptane can have surfaces tensions near 20 mN/m, but the conductivity is orders of magnitude lower.

d. Surfactants. While many systems have added ionic and acidic compounds to modify the conductivity, very few systems have surfactants added to modify surface tension. In the work of Smith,[55] one of the liquids used was water (doped with NaCl for conductivity changes) that had 0.5% "Hodag 1035L" surfactant added to lower the surface tension, which seems to be well in excess of the critical micelle concentration (CMC);[66] no mention was made of any possible Marangoni stresses resulting from the addition of surfactant. Hodag is listed as a nonionic surfactant and only lowers the air-water surface tension to $\sim$50 mN/m. The other report of using surfactant is by Hayati *et al.*,[67] who added an ionic surfactant "AOT" to hexadecane to adjust the conductivity of the sprayed liquid (hexadecane), but there is no mention of its effect on surface tension variation. Only recently,[68] an attempt to systematically investigate the effect of surfactants on the cone-jet mode in liquid-liquid electrosprays was made. The properties of the fluid used in that study,[68] which are of interest here, correspond to (a) the greater than one viscosity ratio of the dispersed to that of the external fluid, $\mu_i/\mu_o > 1$, which is opposite to our case, (b) lower than our conductivity, $\kappa < O(0.1\,\mathrm{S/m})$, and (c) higher than our interfacial tensions. According to this work,[68] the addition of surfactant below the CMC for the high conductivity case (closest to our study) does not appear to modify ES properties appreciably. However, above the CMC, no typical cone-jet mode is found, but instead one observes thicker unstable jets (compare to our larger emitted droplets), reduced dependence of current on flow rate, higher currents than expected from standard ES theory (versus our lower currents), and droplet diameter increase with decreasing interfacial tension. Although some of these observations are not consonant with ours, it is clear that an electrical current transport mechanism for high surfactant concentrations must be different from that in the classical ES and the surfactant distribution along the interface is non-uniform.

e. Summary. The above discussion suggests that our system possesses properties far different from any electrospray system reported in the literature, as summarized in Figure 14. Finally, a few other physical aspects differentiating CRDTS from Taylor cones are worth mentioning. While electrified liquid cones have been studied since the early work of Zeleny,[71,72] who dealt with a variety of electrolytes held at the tip of a capillary in a gas at atmospheric pressure, until the 1960s most work focused on the behavior of perfect conductors, (mercury or water) or perfect dielectrics (apolar liquids such as benzene) and later on poorly conducting liquids—leaky dielectrics—by Allan and Mason.[73] However, there are significant differences between the behavior of electrolytes[74–76] and leaky dielectrics. In electrolytes, electrokinetic phenomena are dominated by effects of interface charge derived from covalently bound ionizable groups or ion adsorption. Near a surface charged in this fashion, a diffuse charge cloud forms as electrolyte ions of opposite charge are attracted toward the interface. A concentration gradient forms so that diffusion balances electromigration. Then, when a field is imposed, processes in this diffuse layer govern the mechanics. With perfect conductors, perfect dielectrics, or leaky dielectrics, diffuse layers associated with equilibrium charge are usually absent. Nevertheless, the underlying processes share many characteristics. Most obvious is that electric charge and current originate with ions. Liquid metal TC are most singular because the very high conductivity of liquid metals $\kappa \sim 10^6\,\mathrm{S/m}$ leads to the formation of exceedingly sharp tips, which may emit predominantly single ions with very little company of larger clusters. Taylor cones in their original embodiment in atmospheric pressure gases are commonly referred to as "electrosprays." Taylor cones of metals and nonmetals behave quite differently near their onset conditions. For electrolyte spraying from a DC Taylor cone, ions from the bulk electrolyte are transported and concentrated at the tip to drive a Rayleigh fission process. Spraying of dielectric liquid via DC Taylor cones is also possible, but it requires significantly higher voltages and is believed to be driven by the momentum and mass flux of an ion evaporation

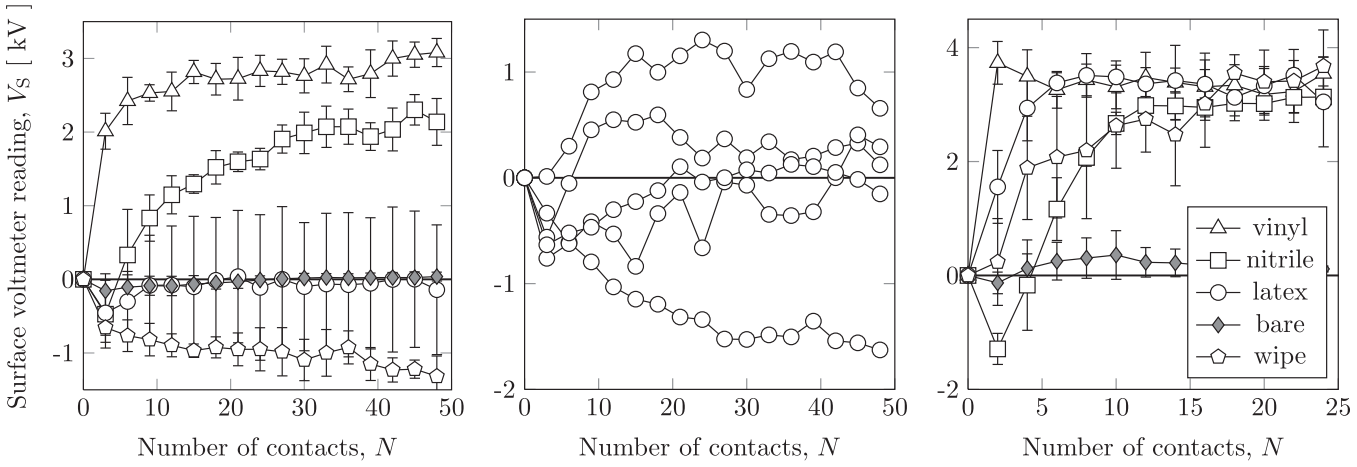

(a) Normal contact (all materials). (b) Normal contact (latex only). (c) Sliding contact (all materials).

FIG. 15. Measurements of surface potential resulting from contact electrification. (a) Repeated normal contact of the polystyrene cuvette sidewall with several glove materials and a laboratory wipe (labeling is shown in (c)) produces a range of surface voltages both in magnitude and polarity. Each data point is the average of five measurements for a different cuvette. The error bars indicate the standard deviation about the average. For vinyl and the laboratory wipe, the magnitude of the voltage increases with contact, whereas for nitrile, the cuvette first obtains a negative charge followed by a reversal to positive polarity. Contact with a bare finger produces an insignificant charge. The data for latex are deceptive in that the average for the five runs is near zero. However, the error bars indicate a wide variation in charge level and polarity. As shown in (b), different experimental runs produced positive, negative, and nearly zero polarity on the surface of the cuvette. This irreproducibility is an often-cited characteristic of contact electrification of insulators,[30] but we observe it here for latex only. (c) Repeated sliding contact yields larger values of V_S (compared to normal contact) and a change to positive polarity in the case of the laboratory wipe.

process at the cone tip.[77] Another obvious difference between Taylor cones in metals and electrolytes is that charge emission in the former is dominated by field evaporation,[78] while this mechanism rarely plays a role in electrolytes, which are studied in the presented work. Thus, the combined differences in fluid properties (viscosity ratio, conductivity, and surface tension), the presence of surfactants, and the electrolyte characteristics of the sprayed fluid contribute to the drastic contrast between CRDTS and traditional electrosprays.

IV. CONCLUSIONS

In this paper, we have uncovered the true nature of chemical reaction-driven tip-streaming as first reported by Fernandez and Homsy[15] and have found that, although peculiar, it was not a self-sustaining droplet formation phenomenon as previously thought. It is clear now, after a systematic experimental investigation involving careful observations and measurements, that the phenomenon is really initiated and sustained by electric forces resulting from contact electrification of the experimental apparatus. Coincidentally, the original experiments of Fernandez and Homsy employed materials (plastics and rubbers) that can easily acquire charge with minimal contact and the oil-water-surfactant chemistry is such that the water phase is highly conductive and the interfacial tension can achieve extremely low values. Perhaps if the dynamic interfacial tension measurements of Fernandez and Homsy,[15,26] which led to their observations, had been accomplished using an inverted oil-acid droplet immersed in the water-alkali solution—a setup employed by Touhami *et al.*[27] for measurements of the same chemical system—the CRDTS phenomenon would have never been discovered. In retrospect, without knowing that static charge was present on the experimental apparatus coupled with the presence of surfactant and observed motion, it was only logical that Marangoni effects are solely responsible for the phenomenon—the present study does point out their major influence, which differentiates CRDTS from standard ES. All the studies of CRDTS to date,[15,19,23] including the present one, lead to the key intriguing question—while in the present experiments, Marangoni stresses alone cannot maintain tip-streaming, the theory by one of the authors[23] proves the possibility of the existence of tips-streaming driven purely by Marangoni effects, which is yet to be discovered experimentally.

ACKNOWLEDGMENTS

The authors would like to thank UCSB Mechanical Engineering undergraduate Ruben Diaz, supported by California Alliance for Minority Participation (CAMP) program, for help in the laboratory at the start of this project in 2010, and Professor Bud Homsy for his encouragement at the 2010 APS-DFD conference, where the key findings were presented. This work was partially supported by the National Science Foundation (NSF) CAREER award under Grant No. 1054267 and American Chemical Society (ACS) Petroleum Research Fund under Grant No. 51307-ND5.

APPENDIX A: CHARGE MEASUREMENTS ON CUVETTE SIDEWALLS

Prior to exploring the surface potential relative to the tip of the capillary resulting from contact electrification, it was measured on a set of un-handled cuvettes,[79] i.e., those that were not touched by gloved or bare hands between the time of purchase and the time of measurement. The cuvettes were

transferred to the holder, cf. (D) in Figure 4, using fine tip stainless steel tweezers to minimize contact. Measuring voltage on each of the four vertical sides of 22 cuvettes (88 measurements) resulted in an average surface voltage of $V_S = -165 \pm 60\,\text{V}$ for the un-handled cuvettes. This initial charge present on the cuvettes may be due to contact with the styrofoam packaging container and/or particularities of the manufacturing process.

Confirming whether a significant charge can be transferred by contact electrification during handling of the cuvettes required measurements of surface potential on cuvette sidewalls after repeated contact with gloved hands and laboratory wipes (i.e., under the conditions which likely occurred during the original experiments of FH[80]). For these experiments, two types of contact were employed. The first, which we will call "normal" contact, was produced by simply touching the side of the cuvette with an index finger and removing the finger in a direction nearly perpendicular to the surface with as little sliding motion as possible. The second, which we will call "sliding" contact, was achieved by sliding the index finger down the side of the cuvette. It is anticipated that actual contact, where the experimenter is not interested in monitoring their handling, is a combination of normal and sliding contact motions. The number of sequential contacts made with the cuvette is denoted by N. Due to the manual nature with which we are producing contact, there will undoubtedly be variations in contact area, force, and sliding distance between different contact events. However, simple measurements using a laboratory balance indicate that the force imparted by the index finger is around $\sim 1 - 5\,\text{N}$ and the normal contact area to be around $\sim 1.5\,\text{cm}^2$, which corresponds to a contact pressure of $\sim 10 - 50\,\text{kPa}$. For sliding, however, the contact area is a significant fraction of the sidewall area (i.e., $\sim 4\,\text{cm}^2$). The normal and sliding contact experiments were performed with a variety of glove materials including latex (MF-300, MicroFlex®), nitrile (KC500, Kimberly-Clark®), and vinyl (#96-234, Oak Technical) as well as laboratory wipes (KimWipes, Kimberly-Clark®) and bare skin (an un-gloved index finger). The results of these measurements are shown in Figure 15.

Several key conclusions can be made from the data in Figure 15. First, the magnitudes of the surface potential V_S measured for the various cases of sliding and normal contact are in the range of several kilovolts, which are significantly larger than the initial potential of the cuvette sidewalls, and are consistent[81] with the magnitudes measured in contact electrification experiments by other authors using latex and PTFE samples.[82] Second, there is also consistency between the predicted polarity of charge transfer measured for normal contact (cf. Figure 15(a)) and the order of materials in the triboelectric series of Table I—glove materials producing positive polarity on the cuvette sidewalls while laboratory wipes producing negative polarity.

By comparing Figures 15(a) and 15(c), it is apparent that sliding contact produces larger values of surface potential than normal contact, which could be caused by the increased contact area during the sliding motion. This is also consistent with findings in the literature suggesting that sliding contact results in a higher magnitude of charge transfer as compared to rolling[83] contact, and that the action of rubbing enhances contact charging.[30] And for both normal and sliding contact, it is observed that in general, V_S increases with the number of contacts N, but then tends to plateau. This trend is reminiscent of recent contact electrification experiments using the insulator particle desorption mass spectrometry (PDMS)[84] that reported the same general behavior.

There are a few more peculiarities of the contact electrification experiments: the apparent reversal of charge polarity for certain materials after a low number of contacts (cf. nitrile data in Figures 15(a) and 15(c)), and the sporadic readings for the latex glove material (cf. Figure 15(b)) suggesting both positive and negative charge transfer. Perhaps it is best to consider these to be the result of the complicated frictional charging process or inconsistencies in the latex material from glove-to-glove.[85] From the standpoint of eliminating static charge buildup on the cuvette sidewalls, the data of Figures 15(a) and 15(c) suggest that it would be best to handle the cuvettes with bare hands. The insignificant surface potential readings for bare skin are likely the result of the natural moisture and mineral content of human skin, increasing the surface conductivity of the polystyrene and allowing for more rapid surface discharge during the contact process. However, this goes against good laboratory practice given the sensitivity of liquid interfaces to contamination with surface active impurities.

In summary, it is clear from the data of Figure 15 that only a few contacts ($N \leq 10$) with either gloved fingers or laboratory wipes during normal or sliding contact (consistent with what would be expected of typical handling of cuvettes during experiments), can develop a substantial surface potential on the cuvette sidewalls, which in turn implies strong electric fields in the vicinity of the pendant drop within the cuvette. Also, it must be noted that the measured decay of the surface potential is relatively slow, as shown in Figure 16, which is typical of insulating materials[86] and suggests that the substantial surface potential produced by contact

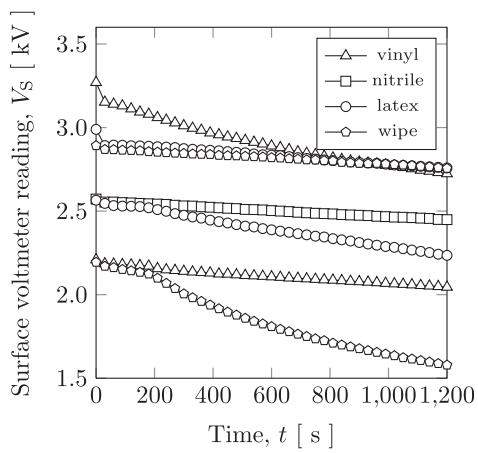

FIG. 16. Charge decay measurements for cuvettes contacted with vinyl, nitrile, latex, and kimwipes. The data suggest that charge decay is relatively slow—a characteristic of insulator surfaces, and that over the course of 20 min (1200 s), the level of charge is still significant (greater than ~70 % of the initial surface voltage). Relative humidity during the course of all surface voltage measurements was in the range 39%–55% RH (no specific correlation between these humidity levels and decay rate was observed).

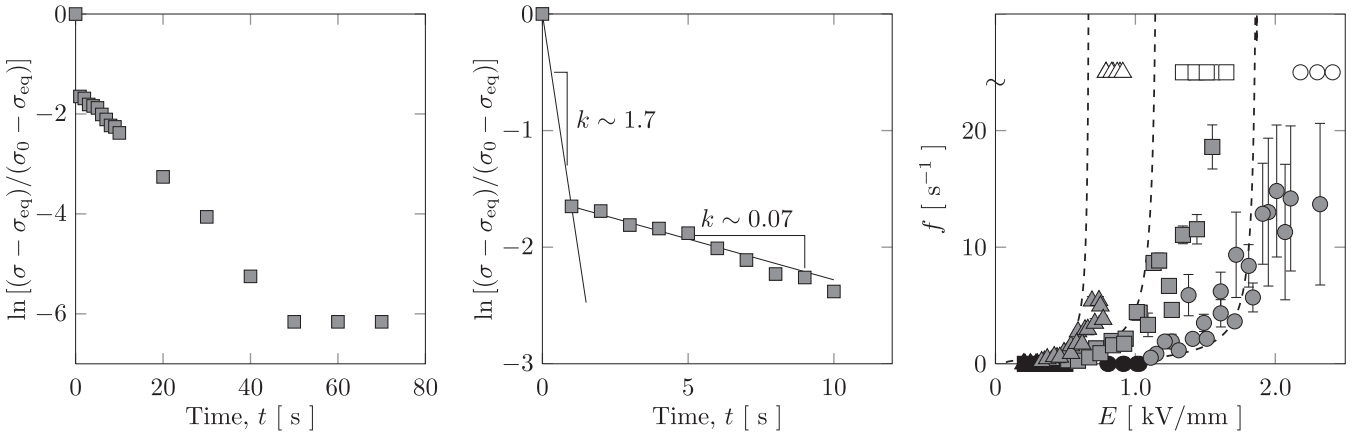

(a) Data for FH system. (b) Detail of (a) showing fits for k. (c) Data and model comparison.

FIG. 17. Short- and long-time reaction rate k values based on the Touhami *et al.*[27,87] data. (a) Data for $C_{\mathrm{NaOH}} = 12.5\,\mathrm{mM}$ and $C_{\mathrm{acid}} = 1.0\,\mathrm{mM}$. (b) Shorter time details of data from (a) showing the short- and long-time estimates of k. (c) Comparison of the measured data from Figure 9 with the results of the model (10) using the values of k_{s}. Note the reasonable quantitative agreement for low frequencies.

electrification can exists over the timescales of 10-20 min associated with the CRDTS phenomena originally reported by FH.

APPENDIX B: ON ESTIMATING THE VALUES OF THE REACTION RATE CONSTANT *K* AND ITS EFFECT ON MODEL (10)

The alkali-acid reaction used in our experiments to form surfactants is often considered to be a first order chemical reaction, cf. Eq. (9), and from published values of $\sigma(t)$ (Refs. 27 and 87), the reaction rate k can be determined, cf. Table III.

Figures 17(a) and 17(b) represent the Touhami *et al.*[27,87] data and show how the choice of the linoleic acid only equilibrium interfacial tension for the initial value can lead to a short-time reaction rate constant k_{s}, cf. Table III. The fitting procedure follows that of Fernandez and Homsy,[26] but here we extend it to estimate the reaction rate for short time, k_{s}, as exemplified in Figure 17 for $C_{\mathrm{NaOH}} = 12.5\,\mathrm{mM}$ and $C_{\mathrm{acid}} = 1.0\,\mathrm{mM}$.

Given these new values of the reaction rate constant, k_{s}, we can evaluate its effect on model (10). First note that model (10) assumes that the interfacial tension varies with time according to Eq. (9), but remains uniformly distributed along the interface. However, given the observed motion in the oil phase, directed from the pendant drop base to its tip, we can anticipate that surfactant is swept towards the tip. It is, therefore, reasonable to expect that the tip region, where droplet emission occurs, becomes crowded with surfactant beyond that suggested by (9). Hence, similar to forcing the transition of $E/E_{\mathrm{TC}} = 1$ for the pulsed cone-jet to cone-jet modes using $\sigma_{0,\mathrm{eff}}$ (cf. Sec. III C 2), we tune model (10) to better match the transition from the deformation only to pulsed cone-jet modes, cf. Figure 9(a). To achieve this, we use new values of σ_{eq} calculated based on $E_{\mathrm{n,min}}$ from Figure 9(a), which are $\sigma_{\mathrm{eq}} = 9$, 2, and $0.1\,\mathrm{mN/m}$ for $C_{\mathrm{acid}} = 0.1$, 1.0, and $10\,\mathrm{mM}$, respectively. Along with $\sigma_{0,\mathrm{eff}}$ and k_{s}, these values are used in Eq. (10) to arrive at the curves in Figure 17(c), which better fit the measured data compared to the solid curves in Figure 9(b). Also note that the *magnitude* of f is dictated by k_{s}.

APPENDIX C: ELECTRIC FIELD AND SPRAY STRUCTURE

1. Electric field

The electric field for our capillary-plane configuration can be approximated by an infinite earthed plane and a semi-infinite line of charge.[88,89] In our case, the line of charge is the capillary held at potential V_0 above the grounded electrode, cf. inset of Figures 8 and 18(a). The separation distance is z_0 (see inset of Figure 8 for the coordinate system). The r- and z-components of the electric field are given by

$$E_r = \frac{V_0}{r\ln(4H/R_{\mathrm{c}})}\left[\frac{2H-z}{\sqrt{r^2+(2H-z)^2}} - \frac{z}{\sqrt{r^2+z^2}}\right],$$

$$E_z = \frac{V_0}{\ln(4H/R_{\mathrm{c}})}\left[\frac{1}{\sqrt{r^2+(2H-z)^2}} + \frac{1}{\sqrt{r^2+z^2}}\right],$$

respectfully, from which one can immediately see that

(1) Both the radial and axial electric field components are functions of r and z. However, for any value of z, the radial component E_r decreases rapidly owing to the r^{-1} factor; furthermore, the radial component E_r decreases rapidly in the z direction beyond $z > R_{\mathrm{c}}$.
(2) The axial component E_z of the electric field decays with radial position, but less rapidly than E_r, as well as it decays with the distance z from the needle, cf. Figure 18(b).

2. Spray structure

The phenomenon of the ordered droplet splitting, i.e., when one drop goes to the right and the next one to the left, cf. Figure 1(e), was treated in KH as the Marangoni driven flow solution could not account for a wide cone angle of the spray structure. Under the belief that drop formation was

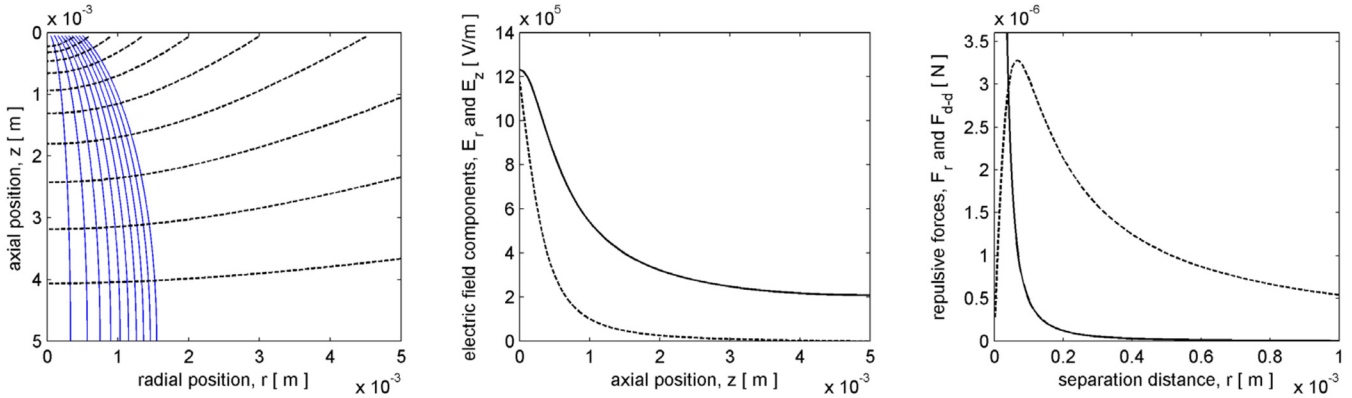

(a) Plot of electric field lines (solid) and isopotentials (dashed) between the needle and grounded plane electrode.

(b) Decay of E_z (solid) and E_r (dashed) with axial position z; plotted values are for $r = R_c = 0.45\,\text{mm}$.

(c) Comparison of F_{d-d} (solid) and F_r (dashed) for conditions in the neighborhood of the needle.

FIG. 18. Electric field and interaction forces associated with its presence; the plots are generated using the experimental values for the needle voltage (2000 V), needle radius, and the needle-electrode separation distance.

only Marangoni driven, it was assumed that there was no externally imposed flow and no net droplet charge, and thus double layer repulsion between small droplets and the large drop could be responsible for the observed droplet splitting structure. It is now clear, however, that the droplet motion will be influenced by interaction (repulsion) between charged droplets and movement of charged droplets in the radial and axial directions owing to the presence of the electric field, which is discussed in detail in Appendix C1.

It is apparent that the highest electric field strength will be in the vicinity of the capillary tip. The magnitude of E_r and E_z at this location is given by $E_z \sim E_r \sim V_0/(R_c \ln(4z_0/R_c))$, so that the forces in the radial and axial directions can be computed by $F_r = q_d E_r$ and $F_z = q_d E_z$ (where q_d is the charge on the droplet). Very near the tip of the capillary, the axial and radial forces are of the same order of magnitude—thus we could expect a rather wide "spray cone" angle. However, we do not observe nearly the same radial velocity as the axial velocity near the needle tip in our experiments for two primary reasons. First, the radial field decays very rapidly in both the r and z directions. Second, the radial electric field is zero along the axis ($r = 0$) in the vicinity of the drop tip where the droplets are produced. Accordingly, we do not expect radial velocities to be as large as axial velocities in the neighborhood of the needle tip.

For the sake of an estimate, let us use the Rayleigh charge limit for the droplet charge, i.e., $q_d \sim q_R = 8\pi(\epsilon_{r,oil}\,\epsilon_0\,\sigma\,r^3)^{1/2} \sim 10^{-12}\,\text{C}$, though the actual charge will be some fraction of this.[90] With this value, we can estimate the axial and radial forces on the droplets in the electric field. For the parameter values from our flow visualisation experiments (i.e., $R_c = 0.45\,\text{mm}$, $z_0 = 10\,R_c, V_0 = 2000\,\text{V}$, and $q_d \sim 10^{-12}\,\text{C}$), we find that $F_z \sim 1.2 \times 10^{-6}\,\text{N}$. To compare this to our experiments, we can equate this force to the Stokes drag, $F_{St} = 6\pi\mu r U$ and determine the expected droplet velocity $U_z \sim 15\,\text{mm/s}$, which is of the same order of magnitude as the measured droplet velocities near the tip of the interface. This estimate is valid for a drop moving in a stationary fluid: hence, if we consider this velocity relative to a moving fluid (e.g., the moving oil in the vicinity of the

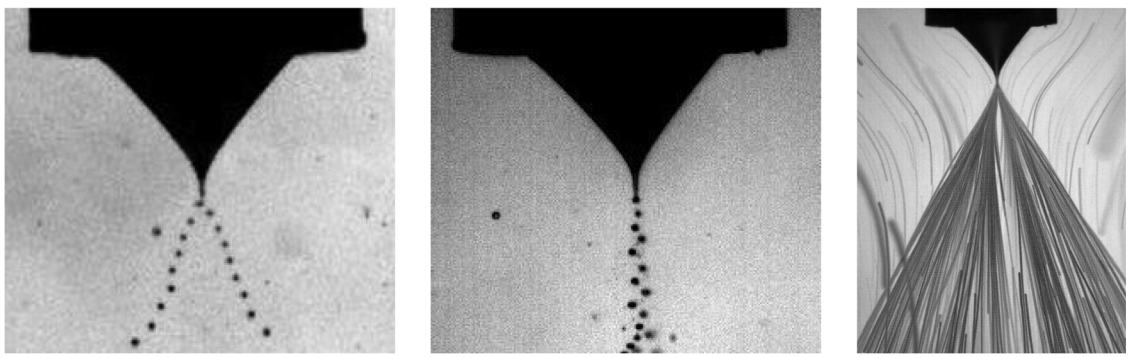

(a) Front view.

(b) Side view.

(c) Superimposed images.

FIG. 19. Images of the cone-jet spray structure using two high-speed cameras positioned 90° apart to obtain simultaneous front and side views (shown for conditions of $V = 2000\,\text{V}$ and $H/R_c \sim 10$). (a) A single frame from high-speed movie recorded at 4000 fps showing droplet splitting near the tip. (b) Simultaneously, another camera records the motion of the droplets from an angle orthogonal to (a). The spray structure captured in (a) and (b) suggests that near the tip the droplets are confined to a nearly 2D plane as they move away from one another. This behavior can be attributed to our spray having a low droplet density (due to low formation frequency). The dominant interaction near the tip occurs between droplet pairs, hence the spreading within more or less a plane. (c) With time, this plane of droplets rotates, so that a superposition of images (1000 frames representing 0.25 s) appears as an axisymmetric cone spray.

interface as observed in the experiments), the value of U_z would be larger. Knowing that the axial field strength decreases with distance from the needle, the axial droplet velocity will decrease, e.g., taking $z = z_0/2$ corresponding to $\sim$2.5 mm from the needle tip in our experiments, the axial force on the droplet decreases by nearly one half with a similar change in the velocity computed using Stokes drag, which is also consistent with experimental observations, cf. Figure 18(c).

Finally, why do the droplets split apart as observed in Figure 1(f)? There is also the droplet-droplet repulsion force as a result of the droplet charge, which can be represented as $F_{\mathrm{d-d}} = q_{\mathrm{d}}^2/(4\,\epsilon_{\mathrm{r,oil}}\,\epsilon_0\,r^2)$, where r is now the distance between droplets. This force can be quite substantial at small separation distances—with the highest forces occurring near the point of droplet formation. As an example of the magnitude, consider that $r = 2$ d, which gives $F_{\mathrm{d-d}} \sim 2.2 \times 10^{-6}$ N. Thus, the droplet-droplet repulsive force could be the mechanism that initially repels (splits) the droplets away from the axis. This expectation is supported by a direct observation of the spray shown in Figures 19(a) and 19(b), which clearly indicate that near the tip, the droplets are confined to a nearly two-dimensional plane as they move away from one another. The observed behavior can be attributed to our spray having a low droplet density (due to low formation frequency), so that the relatively fast moving droplets do not have enough time to rearrange themselves in an optimal three-dimensional spiral-type structure. However, as suggested by Figure 19(c), with time this plane of droplets rotates so that a superposition of images appears as an axisymmetric cone spray.

[1]E. R. Lee, *Microdroplet Generation* (CRC Press, 2002).
[2]O. A. Basaran, "Small-scale free surface flows with breakup: Drop formation and emerging applications," AIChE J. **48**, 1842–1848 (2002).
[3]G. M. Whitesides, "The origins and the future of microfluidics," Nature **442**, 368–373 (2006).
[4]A. B. Theberge, F. Courtois, Y. Schaerli, M. Fischlechner, C. Abell, F. Hollfelder, and W. T. S. Huck, "Microdroplets in microfluidics: An evolving platform for discoveries in chemistry and biology," Angew. Chem., Int. Ed. **49**, 5846–5868 (2010).
[5]A. Huebner, S. Sharma, M. Srisa-Art, F. Hollfelder, J. B. Edel, and A. J. deMello, "Microdroplets: A sea of applications?," Lab Chip **8**, 1244–1254 (2008).
[6]Y. Xia and G. M. Whitesides, "Soft lithography," Annu. Rev. Mater. Sci. **28**, 153–184 (1998).
[7]N. T. Nguyen and S. T. Wereley, *Fundamentals and Applications of Microfluidics* (Artech House, Boston, 2006).
[8]H. A. Stone, "Dynamics of drop deformation and breakup in viscous fluids," Annu. Rev. Fluid Mech. **26**, 65–102 (1994).
[9]J. B. Fenn, M. Mann, C. K. Meng, S. F. Wong, and C. M. Whitehouse, "Electrospray ionization for mass spectrometry of large biomolecules," Science **246**, 64–71 (1989).
[10]G. Loscertales, A. Barrero, I. Guerrero, R. Cortijo, M. Marquez, and A. M. Gañán-Calvo, "Micro/nano encapsulation via electrified coaxial liquid jets," Science **295**, 1695 (2002).
[11]O. V. Salata, "Tools of nanotechnology: Electrospray," Curr. Nanosci. **1**, 25–33 (2005).
[12]S. B. Sample and R. Bollini, "Production of liquid aerosols by harmonic electrical spraying," J. Colloid Interface Sci. **41**, 185–193 (1972).
[13]J. P. Borra, Y. Tombette, and P. Ehouarn, "Influence of electric field profile and polarity on the mode of ehda related to electric discharge regimes," J. Aerosol Sci. **30**, 913–925 (1999).
[14]L. Yeo, D. Lastochkin, S.-C. Wang, and H.-C. Chang, "A new ac electrospray mechanism by Maxwell-Wagner polarization and capillary resonance," Phys. Rev. Lett. **92**, 133902–133904 (2004).
[15]J. M. Fernandez and G. M. Homsy, "Chemical reaction-driven tip-streaming phenomena in a pendant drop," Phys. Fluids **16**, 2548–2555 (2004).
[16]For clarity of the discussion, we refer to the emitted drops as *droplets* and to the drop pendant on the capillary as *drop*.
[17]This chemical combination has been used as a model system for caustic/alkali flooding, a type of enhanced oil recovery technique where alkalis are added to an injected water phase to react with organic acids naturally found in crude oil (Refs. 91 and 92).
[18]C. I. Chiwetelu, V. Hornof, and G. H. Neale, "Interaction of aqueous caustic with acidic oils," J. Can. Pet. Technol. **28**, 71–78 (1989).
[19]R. Krechetnikov and G. M. Homsy, "On physical mechanisms in chemical reaction-driven tip-streaming," Phys. Fluids **16**, 2556–2566 (2004).
[20]G. I. Taylor, "The formation of emulsions in definable fields of flow," Proc. R. Soc. London, Ser. A **146**, 501–523 (1934).
[21]R. A. de Bruijn, "Tipstreaming of drops in simple shear flows," Chem. Eng. Sci. **48**, 277–284 (1993).
[22]S. L. Anna and H. C. Mayer, "Microscale tipstreaming in a microfluidic flow focusing device," Phys. Fluids **18**, 121512 (2006).
[23]R. Krechetnikov, "Structure of Marangoni-driven singularities," Phys. Fluids **24**, 022111 (2012).
[24]G. I. Taylor, "Disintegration of water drops in an electric field," Proc. R. Soc. London, Ser. A **280**, 383–397 (1964).
[25]T. Ward, M. Faivre, and H. A. Stone, "Drop production and tip-streaming phenomena in a microfluidic flow-focusing device via an interfacial chemical reaction," Langmuir **26**, 9233–9239 (2010).
[26]J. M. Fernandez and G. M. Homsy, "Viscous fingering with chemical reaction: Effect of *in-situ* production of surfactants," J. Fluid Mech. **480**, 267–281 (2003).
[27]Y. Touhami, V. Hornof, and G. H. Neale, "Dynamic interfacial tension behavior of acidified oil/surfactant-enhanced alkaline systems—1. Experimental studies," Colloids Surf. A **132**, 61–74 (1998).
[28]In the report of FH, it was unclear whether or not the diameter or radius of the needle used in their experiments was 0.5 mm. An earlier FH paper (Ref. 26) (upon which the CRDTS work is based) is of no help as they do not report the needle size used, and our attempt to estimate the needle diameter based on the published pendant drop images gives a value of $\sim$2 mm.
[29]In their paper (Ref. 15), FH do not mention static charge-related behavior during the course of experiments. In the companion paper (Ref. 19), the apparent similarity between the cone shape of the water-alkali pendant drop in the CRDTS experiments and the shape of a Taylor cone is pointed out, but due to a lack of evidence of static charge and obviously no imposed electric field in the experiments, there was no pursuit of such an explanation.
[30]D. J. Lacks and R. M. Sankaran, "Contact electrification of insulating materials," J. Phys. D: Appl. Phys. **44**, 453001 (2011).
[31]When we say that charge is transferred, we are not implying that charge is created—instead, one material becomes positively charged while the other becomes negatively charged, i.e., there is some mechanism responsible for charge acquisition. The mechanism for insulators still remains elusive (Ref. 30), unlike metal-to-metal contact electrification in which both the magnitude and polarity of charge transfer is related to the difference in work functions between materials. For insulators, it is proposed that there could be three different means by which charge is carried from one material to the other. These are (Ref. 30) (a) electron transfer between materials, (b) surface ions transferred as a result of contact, and (c) surface material transfer (e.g., literally small patches of surface material). Thus, although we do not know, in the case of the materials used in the CRDTS experiments, which mechanism is responsible for charge transfer, it is clear that after contact and separation, the two insulator surfaces have acquired charges of opposite polarity.
[32]Material properties include the chemical composition of the surface (i.e., different insulators such as PTFE, Perspex, and glass can charge differently under the same conditions (Ref. 86)) and pre-treatment or cleaning procedures for the surfaces. Environmental conditions such as ambient pressure, temperature, and humidity are known to have dramatic effects. For example, surface charge decay (the rate of discharging) is known to be influenced by humidity, through the presence of surface water layers (Ref. 93). These water layers, which are formed from adsorbed water molecules present in air, can act as charge carriers because of the disassociation of water molecules into ionic species. Finally, the contact process itself can lead to differences in contact electrification. It has been demonstrated that the nature of contact between materials (e.g., sliding motion versus rolling motion) can affect charge transfer magnitude and polarity (Ref. 83) as can variations in the contact force (Ref. 94), area (Ref. 84), and the number (Ref. 84) or history (Ref. 41) of contacts between material samples.

[33]G. R. Freeman and N. H. March, "Triboelectricity and some associated phenomena," Mater. Sci. Technol. **15**, 1454–1458 (1999).
[34]A. F. Diaz and R. M. Felix-Navarro, "A semi-quantitiative trio-electric series for polymeric materials: The influence of chemical structure and properties," J. Electrostat. **62**, 277–290 (2004).
[35]There is no indication in the original CRDTS paper of FH (Ref. 15) what type of gloves were used during handling of the experimental equipment. However, it is expected that at least some type of gloves was worn as the original observations of the droplet formation behavior were made during the course of dynamic interfacial tension measurements. Such measurements require extreme care and cleanliness to produce accurate results.
[36]As Diaz *et al*. (Ref. 34) pointed out, it is noteworthy that the ordering of polymers between different series is *"remarkably similar."*
[37]S. M. Bystryak and M. A. Winnik, "Unusual conductivity changes for sodium dodecyl sulfate solutions in the presence of polyethyleneimine and polyvinylamine," Langmuir **15**, 3748–3751 (1999).
[38]Y. Y. Akhadov, *Dielectric Properties of Binary Solutions* (Pergamon Press, 1980).
[39]R. M. Hill and J. Lawrence, *Encylopedia of Surface and Colloid Science: Dielectric Spectroscopy of Micro-emulsions* (Marcel Dekker, Inc., 2002).
[40]J. A. Cross, *Electrostatics: Principles, Problems, and Applications* (IOP Publishing Ltd., 1987).
[41]D. M. Taylor and D. R. Owen, "An instrument for measuring static dissipation from materials," J. Electrostat. **19**, 53–64 (1987).
[42]Indeed, note that insulators behave differently from metals (conductors): When a surface voltmeter or any grounded object is brought close to a charged insulator, the proximity will reduce the voltage of the insulator surface in that region. In addition, the voltage varies from place to place across an insulator as opposed to that of a metal surface, which is always the same everywhere.
[43]For finite size sample sizes and separation distances L other than the value of $L_{\text{meas}} = 2.54\,\text{cm}$ recommended by the manufacturer, a correction factor is used to calculate the "actual" surface voltage and surface charge density using the displayed voltage value V_{disp}: $Q/A = V_{\text{disp}}(\epsilon_0/L_{\text{meas}})[f/(f-1)]$, where $f = \sqrt{1 + D^2/(4L^2)}$ and D is the characteristic size of the sample. This equation suggests that the actual voltage directly under sensor is $V_{\text{disp}}f/(f-1)$, i.e., larger than the displayed voltage reading V_{disp} since $f > 1$—this also means that the true charge density Q/A is larger by the factor of $f/(f-1)$.
[44]X. Zhang and O. A. Basaran, "Dynamics of drop formation from a capillary in the presence of an electric field," J. Fluid Mech. **326**, 239–263 (1996).
[45]Note that ranges for the falling velocity U_{fall} and terminal velocity U_{term} are provided. This is due to the discrepancy in needle size reported in the original work of FH that was mentioned in the footnote of Sec. II A.
[46]R. Clift, J. R. Grace, and M. E. Weber, *Bubbles, Drops, and Particles* (Academic Press, Inc., 1978).
[47]M. Cloupeau and B. Prunet-Foch, "Electrostatic spraying of liquids: Main functioning modes," J. Electrostat. **25**, 165–184 (1990).
[48]J. M. Grace and J. C. M. Marijnissen, "A review of liquid atomization by electrical means," J. Aerosol Sci. **25**, 1005–1019 (1994).
[49]M. Cloupeau and B. Prunet-Foch, "Electrohydrodynamic spraying functioning modes: A critical review," J. Aerosol Sci. **25**, 1021–1036 (1994).
[50]Note that moderate conductivity[48] corresponds to $10^{-8} < \kappa < 10^{-4}\text{S/m}$.
[51]A. Ramos and A. Castellanos, "Conical points in liquid-liquid interfaces subjected to electric fields," Phys. Lett. A **184**, 268–272 (1994).
[52]A. Barrero, J. M. Lopez-Herrera, A. Boucard, I. G. Loscertales, and M. Marquez, "Steady cone-jet electrosprays in liquid insulator baths," J. Colloid Inter. Sci. **272**, 104–108 (2004).
[53]A. Barrero, A. M. Gañán-Calvo, J. Dávila, A. Palacios, and E. Gómez-González, "The role of electrical conductivity and viscosity on the motions inside Taylor cones," J. Electrostat. **47**, 13–26 (1999).
[54]I. Hayati, A. I. Bailey, and T. F. Tadros, "Investigations into the mechanisms of electrohydrodynamic spraying of liquids I. Effect of electric field and the environment on pendant drops and factors affecting the formation of stable jets and atomization," J. Colloid Inter. Sci. **117**, 205–221 (1987).
[55]D. P. H. Smith, "The electrohydrodynamic atomization of liquids," IEEE Trans. Ind. Appl. **IA-22**, 527–535 (1986).
[56]Because of the variations in σ_{eq} with acid concentration and the limited output of our high voltage power supply, it became necessary to vary H/R_c in order to obtain both the pulsed cone-jet and cone-jet modes for each of the reagent concentrations.
[57]A. M. Gañán-Calvo, J. Dávila, and A. Barrero, "Current and droplet size in the electrospraying of liquids. Scaling laws," J. Aerosol Sci. **28**, 249–275 (1997).
[58]It must be noted that to our knowledge, no evidence in the literature exists for a direct quantitative comparison between measurements of interfacial velocity for electrosprays and the values from either velocity field calculations or simple estimates (Refs. 53, 67, 95, and 96).
[59]The relaxation oscillator model was found to predict a change in pendant drop oscillation frequency with reaction rate—behavior speculated on by FH but not demonstrated in experiments because only one set of reagent concentrations was used.
[60]E. A. van Nierop, A. Ajdari, and H. A. Stone, "Reactive spreading and recoil of oil on water," Phys. Fluids **18**, 038105 (2006).
[61]I. Hayati, A. I. Bailey, and T. F. Tadros, "Investigations into the mechanisms of electrohydrodynamic spraying of liquids II. Mechanism of stable jet formation and electrical forces acting on a liquid cone," J. Colloid Inter. Sci. **117**, 222–230 (1987).
[62]This "steady-state" value is in agreement with the measurement of FH (Ref. 15) reported for only one observation of steady tip-streaming; however, in general the droplet size varies with electrode voltage and time.
[63]C. D. Eggleton, T. Tsai, and K. J. Stebe, "Tip streaming from a drop in the presence of surfactants," Phys. Rev. Lett. **87**, 048302 (2001).
[64]R. Stocker and J. W. M. Bush, "Spontaneous oscillations of a sessile lens," J. Fluid Mech. **583**, 465–475 (2007).
[65]H. Kim, D. Luo, D. Link, D. A. Weitz, M. Marquez, and Z. Cheng, "Controlled production of emulsion drops using an electric field in a flow-focusing microfluidic device," Appl. Phys. Lett. **91**, 133106 (2007).
[66]As a comparison, consider the surfactant Triton X-100, which has a critical micelle concentration corresponding to ∼0.01 %. Thus, a concentration of 0.5% would be 50 times the CMC.
[67]I. Hayati, A. I. Bailey, and T. F. Tadros, "Mechanism of stable jet formation in electrohydrodynamic atomization," Nature **319**, 41–43 (1986).
[68]A. G. Marin, I. G. Loscertales, and A. Barrero, "Surface tension effects on submerged electrosprays," Biomicrofluidics **6**, 044104 (2012).
[69]V. R. Gundabala, N. Vilanova, and A. Fernandez-Nieves, "Current-voltage characteristics of electrospray processes in mircofluidics," Phys. Rev. Lett. **105**, 154503 (2010).
[70]J. M. López-Herrera, A. Barrero, A. Boucard, I. G. Loscertales, and M. Márquez, "An experimental study of the electrospraying of water in air at atmospheric pressure," J. Am. Soc. Mass Spectrom. **15**, 253–259 (2004).
[71]J. Zeleny, "The electrical discharge from liquid points, and a hydrostatic method of measuring the electric intensity at their surfaces," Phys. Rev. **3**, 69–91 (1914).
[72]J. Zeleny, "Instability of electrified liquid surfaces," Phys. Rev. **10**, 1–6 (1917).
[73]R. S. Allan and S. G. Mason, "Particle behavior in shear and electric fields. I. Deformation and burst of fluid drops," Proc. R. Soc. London, Ser. A **267**, 45–61 (1962).
[74]D. A. Saville, "Electrokinetic effects with small particles," Annu. Rev. Fluid Mech. **9**, 321–337 (1977).
[75]D. A. Saville, "Electrohydrodynamics: The Taylor-Melcher leaky dielectric model," Annu. Rev. Fluid Mech. **29**, 27–64 (1997).
[76]W. B. Russel, D. A. Saville, and W. R. Schowalter, *Colloidal Dispersions* (Cambridge University Press, Cambridge, 1989).
[77]M. Gamero-Castano and J. Fernandez de la Mora, "Kinetics of small ion evaporation from the charge and mass distribution of multiply charged clusters in electrosprays," J. Mass Spectrom. **35**, 790–803 (2000).
[78]J. Fernandez de la Mora, "The fluid dynamics of Taylor cones," Annu. Rev. Fluid Mech. **39**, 217–243 (2007).
[79]The polystyrene cuvettes were purchased in quantities of 100 per box. In their original packing, the cuvettes are contained in a styrofoam box and completely separated from contacting one another. If the cuvettes in the original experiments had been purchased at a stockroom, they may have been removed from these containers with gloved or bare hands.
[80]For example, if the cuvettes were transported and handled with gloved hands and if the cuvette sidewalls were wiped to eliminate dust or liquids.
[81]Despite the limitations of our static charge measurements, the found values are supported by the following facts. First, the measured surface voltages are comparable to latex-latex contact electrification experiments (Ref. 82) that used a surface voltmeter with a smaller sensor area (2 mm diameter) and separation distance (2 mm). Second, the surface charge density estimated calculated from our surface voltage measurements ($Q/A \sim 8 \times 10^{-10}\,\text{C/m}^2$) are well below the maximum surface charge density based on the maximum surface electric field before breakdown of the air $(Q/A)_{\max} \sim 3 \times 10^{-7}\,\text{C/m}^2$. Third, using a measured surface voltage of $V_S \sim 2000\,\text{V}$, and the equations provided by the manufacturer, we can expect a surface charge density of approximately $8 \times 10^{-10}\,\text{C/cm}^2$.

This is in agreement with PDMS-PDMS contact experiments (Ref. 84) where a Faraday cup was used to measure the total charge on contacted samples. Their results indicate that for 10 contacts the PDMS surface charge density was $\sim 3 \times 10^{-9}\,\mathrm{C/cm^2}$.

[82]M. Sow, R. Widenor, A. Kumar, S. W. Lee, D. J. Lacks, and R. M. Sankaran, "Strain-induced reversal of charge transfer in contact electrification," Angew. Chem., Int. Ed. **51**, 2695–2697 (2012).

[83]R. Elsdon and F. R. G. Mitchell, "Contact electrification of polymers," J. Phys. D: Appl. Phys. **9**, 1445–1460 (1976).

[84]M. M. Apodaca, P. J. Wesson, K. J. M. Bishop, M. A. Ratner, and B. A. Grzybowski, "Contact electrification between identical materials," Angew. Chem. **122**, 958–961 (2010).

[85]It is worth mentioning a comment in the work of Sow *et al*. (Ref. 82), who used latex rubber to explore charge reversal in contact electrification experiments. These authors discovered that charge reversal, resulting from mechanical straining of the samples, was only reproducible for latex rubber purchased from "some manufacturers, but not others."

[86]H. T. M. Haenen, "The characteristic decay with time of surface charges on dielectrics," J. Electrostat. **1**, 173–185 (1975).

[87]Y. Touhami, V. Hornof, and G. H. Neale, "Dynamic interfacial tension behavior of acidified oil/surfactant-enhanced alkaline systems—2. Theoretical studies," Colloids Surf. A **133**, 211–231 (1998).

[88]A. R. Jones and K. C. Thong, "The production of charged monodisperse fuel droplets by electrical dispersion." J. Phys. D **4**, 1159–1166 (1971).

[89]A. M. Gañán-Calvo, J. C. Lasheras, J. Dávila, and A. Barrero, "The electrostatic spray emitted from an electrified conical meniscus," J. Aerosol Sci. **6**, 1121–1142 (1994).

[90]For typical electrosprays, the drop charge is at least half of q_R.

[91]E. H. Mayer, R. M. Weinbrandt, M. R. Irani, and P. H. Krumrine, "Alkaline Waterflooding: Its Theory, Application, and Status," in *2nd European Symposium on Enhanced Oil Recovery* (Editions Technip, Paris, 1982).

[92]A. Satter, G. Iqbal, and J. Buchwalter, *Practical Enhanced Reservoir Engineering* (Pennwell, 2008).

[93]V. Albrecht, A. Janke, E. Nemeth, S. Spange, G. Schubert, and F. Simon, "Some aspects of the polymers' electrostatic charging effects," J. Electrostat. **67**, 7–11 (2009).

[94]H. Sun, H. Chu, J. Wang, L. Ding, and Y. Li, "Kelvin probe force microscopy study on nanotriboelectrification," Appl. Phys. Lett. **96**, 083112 (2010).

[95]V. Shtern and A. Barrero, "Striking features of fluid flows in Taylor cones related to electrosprays," J. Aerosol Sci. **25**, 1049–1063 (1994).

[96]I. Hayati, "Eddies inside a liquid cone stressed by interfacial electrical shear," Colliods Surf. **65**, 77–84 (1992).